OIB/seamount recycling as a possible process for E-MORB genesis

Marc Ulrich, Christophe C Hémond, Philippe Nonnotte, Klaus Peter Jochum

OIB/seamount recycling as a possible process for E-MORB genesis.

Marc Ulrich[1*], Christophe Hémond[1], Philippe Nonnotte[1], Klaus Peter Jochum[2].

Domaines Océaniques, IUEM-UMR 6538, Université de Brest, 29280 Plouzané, France.

Max-Planck-Institut für Chemie, Postfach 3060, D-55020 Mainz, Germany.

* *present address : ISTerre, OSUG-UMR 5275, Université Joseph Fourier, 38000 Grenoble, France*

ABSTRACT

This paper deals with the origin of enriched MORB independent from any hotspot activity. Indeed, MORB enrichment was readily attributed to a ridge/hotspot interaction and in absence of identified neighboring hotspot, to more questionable processes (e.g. incipient plume or plume activity residue). More recently, the existence of enriched MORB away from any identifiable hotspot was attributed to different origins (i.e. recycled oceanic crust and/or enriched mantle after subduction metasomatism). Within this frame, we present here a new set of geochemical analyses of major and trace elements and Sr, Nd and Pb isotopes on samples collected by submersible on both intersections of the 15°20'N fracture zone with the spreading axis of the Mid-Atlantic Ridge. This area is characterized by an increasing enrichment of the lava compositions from north to south through the fracture zone. Results show that the geochemical enrichment observed with a different intensity on both sides of the fracture zone is linked to the 14°N topographic and geochemical anomaly. Our modeling shows that both trace element and isotopic compositions are consistent with a binary mixing between the regional depleted MORB mantle source and a recycled OIB/seamount, as previously proposed to explain the observed enrichment at 14°N [Hémond et al., 2006]. This model can also account for other enriched MORB i.e. the 18°-20°S region of the Central Indian Ridge, illustrating that it does not represent an isolated and local process. On the basis of our results and on the DMM isotopic evolution, the age of the recycled OIB/seamount is estimated to be ~250 Ma, suggesting a recycling within the upper mantle. Considering the huge number of ocean islands and seamounts upon the ocean floor, their recycling into the upper mantle is a plausible process to produce enriched MORB.

1. INTRODUCTION

Over the last 3 decades, the increasing number of oceanographic expeditions together with the development of analytical techniques and the understanding of the mantle-derived basalt composition have allowed us to evaluate the chemical structure of the Earth. In particular, the numerous studies made on mid-ocean ridges basalts (MORB) have led to a classification in groups mainly based on trace element enrichment. Historically, the most abundant ones are depleted and were named “normal” MORB (N-MORB). Compared to basalts from other tectonic environments, N-MORB are characterized by low abundances in incompatible elements, low radiogenic Sr and Pb and high radiogenic Nd (and Hf) isotope ratios [e.g. Hofmann, 1997]. Conversely, enriched MORB [E-MORB; Sun et al., 1979; Schilling et al., 1985] retains their tholeiitic composition but are characterized by more elevated incompatible trace element abundances, trace clement ratios and more radiogenic compositions in Sr and Pb isotopes than N-MORB [Saunders et al., 1988]. E-MORBs have long been considered as a rare expression of MORB, but numerous spreading ridge investigations have demonstrated that MORB enrichment does not represent isolated anomalies [Macdougall and Lugmair, 1986; Zindler and Hart, 1986; Leroex et al., 1992; Cousens et al., 1995; Castillo et al., 1998; Niu et al., 1999]. Therefore, these observations highlight the nature and heterogeneity of the upper mantle beneath mid-ocean ridges.

Although the existence of E-MORB has been known for a long time [Schilling et al., 1985], their origin proves difficult to determine within the binary model of enriched hot spot mantle versus depleted MORB upper mantle. Although some E-MORBs are easily explained by hotspot activity in the vicinity [Schilling, 1973; Schilling et al., 1985], the origin of numerous E-MORB found far away from any obvious plume still remains enigmatic. Along the Mid-Atlantic Ridge, several examples of hotspot-unrelated E-MORB have been described,

among others at 23°N [Donnelly et al., 2004], 14°N [Bougault et al., 1988; Staudacher et al., 1989; Dosso et al., 1991, 1993; Bonatti et al., 1992; Hémond et al., 2006], or 33°S [Michael et al., 1994]. To explain such enrichment, most of the authors have brought up the presence of an enriched component drowned in the "normal" depleted MORB mantle source (DMM), and several possible origins were proposed: old oceanic crust or sediments [Staudacher et al., 1989], an embryonic mantle plume associated with the triple plate junction [Bougault et al. 1988; Dosso et al., 1991], relics of subcontinental mantle [Bonatti et al., 1992], or an unidentified passively embedded chemical heterogeneity in the mantle [Michael et al., 1994]. Nevertheless, none of these have obtained unanimous agreement to explain hotspot-unrelated E-MORB genesis. To account for the origin of E-MORB along the Mid-Atlantic Ridge, Agranier et al. [2005] suggested the dispersion of the "South Hemisphere anomalous mantle" [i.e. the DUPAL anomaly, Dupré and Allègre, 1983; Hart, 1984]. Donnelly et al. [2004] explained that the enrichment observed in one basalt from the Mid-Atlantic Ridge near Kane fracture zone (23°N MARK area) could result from the presence beneath the ridge of a peridotite previously metasomatised by crust-derived enriched melts during subduction. Finally, using trace element concentrations, Hémond et al. [2006] justified the presence of E-MORB at 14°N by recycling beneath oceanic ridges of previously subducted alkali basalts.

In this paper, we present a study of samples recovered on both northern and southern sides of the 15°20'N fracture zone (FZ) during the cruise MODE 98 (R/V Yokosuka, 1998). These samples gave us the opportunity to better constrain the extent of the topographic and geochemical anomaly described at 14°N by Dosso et al. [1991,1993], Bonatti et al. [1992], and Hémond et al. [2006]. By using binary mixing modeling on new trace element and radiogenic isotope (Sr, Nd and Pb) analyzes, this study shows the plausible implication of recycled OIB-type material to the formation of E-MORB not only at 14°N, but also at a global scale.

2. GEOLOGICAL BACKGROUND

The 15°20'N FZ is one of the largest transform faults of the Mid-Atlantic ridge (Fig. 1). The offset is of about 200 km, and the fracture zone 4500 m deep in average. The dextral movement is estimated to 3 $cm.yr^{-1}$ [Charlou et al., 1991; Castillo et al., 1998]. This region is characterized by the presence of enriched MORB [Dosso et al., 1991; Bonatti et al., 1992; Dosso et al., 1993; Hémond et al., 2006] and large but discontinuous ultramafic rock outcrops [Cannat et al., 1997]. These outcrops are not limited to ridge/fracture intersection but extend from 25 km to 35 km on each ridge flank.

The northern segment of the 15°20'N FZ is a complex area with numerous fractures and discrepancies. This segment globally shows slow spreading ridge characteristics, such as a deep axial valley ranging in depth from 3900 m to 4700 m at the intersection with the fracture zone. The ridge flanks are markedly asymmetrical [Cannat et al., 1997]. Ultramafic rocks outcroping north of the 15°20'N FZ are serpentinized peridotites. They have extremely depleted harzburgite-like compositions and represent a high partial melting degree mantle residue [Cannat et al., 1992]. Peridotitic rocks are covered with a thin basaltic layer (< 100 m) locally missing. Basalts crop out in the ridge axis as pillow lavas, tubes or breccia and present fresh glass rims, which are covered by a thin sedimentary layer (< 10 cm). This attests a fairly recent volcanic activity [Cannat et al., 1997].

South of the 15°20'N FZ, harzburgites tectonically crop out in the internal ridge flanks. Basalts are also erupted along the ridge axis, but no sediments are observed, suggesting a higher magmatic activity compared to the northern segment. They are crosscut by decimeter to meter large fissures revealing recent extensive tectonic activity [Cannat et al., 1997]. The entire segment south of the 15°20'N FZ is characterized by a high topographic bulge centered

118 at 14°N [Dosso et al., 1993].

119 In summary, basalts are located near the center of the ridge and seem to result from
120 recent eruptions whereas peridotites and gabbros are exposed on the ridge flanks by a
121 conjugate fault set. Uneven topography is attributed to peridotitic massif uplift across the
122 oceanic crust, associated with intrusive gabbroic bodies, suggesting highly heterogenous
123 lithosphere, both compositionally and mechanically, near the 15°20'N FZ [< 60 km, Escartin
124 and Cannat, 1999]. Away from the fracture zone, the crust is thicker, associated with axis
125 parallel faults and abyssal hills. No peridotite has been dredged, which is consistent with a
126 more homogenous and magmatic crust [Escartin and Cannat, 1999].

127 Samples were picked up using the Shinkaï submersible during the Japanese
128 oceanographic cruise MODE 98 on board the R/V Yokosuka (1998). The samples were
129 collected from the spreading axis and from the intersection massifs between the ridge and the
130 transform fault of both northern (dives 415, 417, 418, 419, 420 and 421) and southern (dive
131 428; Fig. 1) segments.

132

133 **3. ANALYTICAL TECHNIQUES**

134

135 Major element contents were obtained by *in situ* analyses on basaltic glasses by electron
136 probe Camebax SX-50 in Brest, and trace element concentrations using laser ablation sector-
137 field ICP mass spectrometer (laser 213 nm New Wave coupled with Element 2 ICPMS) at the
138 Max-Planck-Institut für Chemie of Mainz [methodology by Jochum et al., 2007]. Sr and Nd
139 fractions were separated using standard ion exchange techniques adapted from Richard et al.
140 [1976] and White and Patchett [1984]. Analyses were performed using a Triton T1 thermal
141 ionization mass spectrometer (TIMS) at the Institut Universitaire Européen de la Mer of the
142 University of Brest; Pb fractions were separated following Manhès et al. [1978] and were

analyzed using a Nu Instrument HR multi-collector ICP-MS at the École Normale Supérieure of Lyon.

Analyses were done on small basaltic glass chips (2-5 mm) carefully selected under a binocular microscope. All chips with apparent sign of alteration or Mn crust were removed. Selected glass chips were leached with 10 mL of HCl 6N at 50°C during 24h. Then, the samples were rinsed twice with distilled water and leachates were saved and analyzed to quantify the effects of the leaching process. Average element concentrations in leachates relative to those of samples do not exceed 8 % for trace elements.

Blanks for Sr, Nd and Pb isotope compositions are respectively 250, 90 and 80 pg and are thus negligible compared to the amount of Sr, Nd and Pb concentrations measured here. Sr (NIST-987), Nd (JNdi-1) and Pb (NIST-981) isotope ratios of reference materials were run with each sample batch. Average results are 0.710241±9 (n=5, ±2σ) for $^{87}Sr/^{86}Sr$ ratio in NBS-987 reference material, 0.512101±9 (n=4, ±2σ) for $^{143}Nd/^{144}Nd$ ratio in JNdi-1 reference material and 16.9327±5, 15.4865±6 and 36.684±2 (n=10, ±2σ) respectively for $^{206}Pb/^{204}Pb$, $^{207}Pb/^{204}Pb$ and $^{208}Pb/^{204}Pb$ ratios in NIST-981 reference material. All these results are consistent with those previously published and available online in the *Geological and Environmental Reference Materials* (GeoReM, http://georem.mpch-mainz.gwdg.de/) database.

4. RESULTS

4.1 Major elements.

Major element data show that our samples are all tholeiitic in composition. It was suggested that major elements in E-MORBs may reveal some variations relative to N-MORBs [*e.g.* increasing content in Al_2O_3 observed in E-MORBs from the MARK area, Donnelly et al., 2004]. This is not the case for the 15°20'N FZ area. No systematic variations can be identified

168 in major elements versus parameters such as latitude or distance to the 15°20'N FZ (*e.g.* Mg#
169 ranges from 41 to 47), except for $Na_{8.0}$ average which decreases from 2.8 for the northern
170 segment to 2.3 for the southern segment.
171
172 **4.2 Trace elements.**
173 Extended trace element patterns (normalized to primitive mantle) [McDonough and Sun,
174 1995] are shown by Figure 2. Basalts from the northern segment are slightly enriched in
175 LREE compared to HREE, with average $(La/Sm)_N$ and $(Dy/Yb)_N$ ratios of 1.10 and 1.07
176 respectively. 418R3 is the only sample that presents higher ratios, with $(La/Sm)_N$ ~1.23 and
177 $(Dy/Yb)_N$ ~1.15. Enrichment for LREE is about 20 to 30 times C1 chondrite contents and less
178 than 20 times for HREE. These samples are therefore intermediate in compositions between
179 N-MORB and more enriched MORB such as basalts from the MARK area or from the MAR
180 14°N anomaly. Extended trace element patterns show slight enrichment in the most
181 incompatible elements with normalized concentrations ranging from 6 to 10 times primitive
182 mantle contents [McDonough and Sun, 1995]. All samples present negative Pb anomalies,
183 which are characteristic of suboceanic mantle [Hofmann, 1988], but also high positive
184 anomaly in Nb-Ta, and negative anomaly in Sr. Generally speaking, the northernmost
185 samples (e.g. 415R4) are less enriched than samples near the fracture zone (e.g. 418R3 ; Fig.
186 3), and follow the geochemical gradient described by Dosso et al. [1991] from 17°10'N to
187 14°N (Fig. 3).
188 Samples patterns from the south of the 15°20'N FZ are sub-identical, indicating that
189 samples probably come from the same magmatic body. These basalts are significantly
190 enriched in LREE with average $(La/Sm)_N$ ratios of ~2. $(Dy/Yb)_N$ ratios are slightly higher than
191 those from the northernmost samples (1.25 *versus* 1.13). Enrichments are also described for
192 strongly incompatible element. Nb-Ta concentrations are 40 times that found in primitive

193 mantle, twice the contents of the most enriched sample from the north segment (418R3).

194

195 **4.3 Sr, Nd and Pb isotope data.**

196 New isotope data presented in this study are plotted in Figure 2 together with isotope
197 data from Atlantic MORB [Agranier et al., 2005]. Considering average isotopic compositions
198 for N-MORB from the North Atlantic of 0.70240, 0.51322, 18.116, 15.463 and 37.68
199 respectively for Sr, Nd and Pb isotopic ratios (averages calculated using MORB away from
200 any hotspot; data are from Agranier et al., 2005], all of our samples presented in this study are
201 more radiogenic in Sr and Pb (and less in Nd) than those of North Atlantic N-MORB. MORB
202 Sr ratios from the northern segment increase from 0.70249 to 0.70265 towards the 15°20'N
203 FZ. The most radiogenic values (~0.70276) are measured on E-MORBs located south of the
204 fracture zone. The dispersion observed in $^{87}Sr/^{86}Sr$ ratios for 415R4, 415R5, 417R1 and 419R4
205 while they are on the mantle array in Nd-Pb and Pb-Pb spaces is likely to be related to
206 seawater interaction. The fact that NAUFARA-007-005 and CHR0077-006-145 samples from
207 Agranier et al. [2005] behave like these four samples also display good evidence for seawater
208 contamination as well. $^{143}Nd/^{144}Nd$ ratios from northern segment samples decrease from the
209 15°20'N FZ to the north. Lower values (~0.512950) are observed in the southern segment
210 samples with isotopic ratio comparable to those of hotspot-related E-MORB (35°N-45°N
211 region related to the Azores hotspot, Turner et al., 1997; Equatorial MAR contaminated by
212 the Sierra-Leone mantle plume, Schilling et al., 1994).

213 MORBs from the northern segment range from 18.3647 to 18.5668 for $^{206}Pb/^{204}Pb$ ratio,
214 from 15.4828 to 15.5075 for $^{207}Pb/^{204}Pb$ ratio and from 37.889 to 38.138 for $^{208}Pb/^{204}Pb$ ratio.
215 Conversely, E-MORBs from the southern segment are characterized by higher isotopic lead
216 ratios, with values about 19.23, 15.56 and 38.86 respectively for $^{206}Pb/^{204}Pb$, $^{207}Pb/^{204}Pb$ and
217 $^{208}Pb/^{204}Pb$. The global increase observed in lead isotope ratios from north to south is in

agreement with the progressive source enrichment through the 15°20'N FZ, as determined by previous trace element and isotope composition analyses (Fig. 3).

5. DISCUSSION

5.1 Enrichment origin.

The statistical study published by Arevalo and McDonough [2009] shows that Atlantic MORBs compared to MORBs from Indian and Pacific oceans are in average more enriched in very incompatible element (e.g. LREE, Ti, Ta, Nb, ...) as well as less incompatible elements (e.g. HREE). To account for this observation, the authors suggested that this enrichment is likely related to smaller degrees of partial melting and/or greater extends of fractional crystallization due to smaller spreading rates, even though the presence of prominent recycled source component or variable proportion of pyroxenite in the Atlantic mantle source is also envisaged. Nevertheless, for the most enriched MORB, it is now commonly accepted that the genesis of E-MORB does not only occur because of smaller degrees of partial melting but requires an enriched source contribution [Dosso et al., 1991; Dosso et al., 1993; Michael et al., 1994; Niu and Batiza, 1997; Donnelly et al., 2004; Hémond et al., 2006; Nauret et al., 2006]. Recent studies on MAR basalts propose that Atlantic MORB heterogeneities have two origins: (1) a long-wavelength character revealing the influence of hotspot mantle *(e.g.* Iceland), and (2) a pervasive shorter wavelength character explained by MORB source contamination with old subducted recycled lithosphere [i.e. the dispersion of the DUPAL anomaly; Dupré and Allègre, 1984; Agranier et al., 2005]. The idea of a hotspot interaction to account for the 14°N anomaly was rapidly abandoned, the nearest hotspot, the Cape Verde islands, being located 1800 km away. Bougault et al. [1988] followed by Dosso et al. [1991] proposed that the 14°N E-MORB may reflect an interaction with an embryonic mantle plume

243 associated with the triple plate junction, but alternative origins of the enriched mantle source
244 was suggested by the same authors shortly after [Dosso et al., 1993]. It was also demonstrated
245 that E-MORBs from the East Pacific Rise (EPR) could be attributed to small discrete blobs of
246 variably fractionated material, with more radiogenic signatures, dispersed as heterogeneities
247 with a size and distribution related to spreading rate at fast spreading ridge [Allègre et al.,
248 1984; Niu et al., 1999]. Thus, it appears that E-MORBs do occur far from any hotspot and
249 without any relationship with deep mantle plumes [Donnelly et al., 2004]. Therefore, when no
250 hotspot is involved, mixing processes between some N-MORB source and some enriched
251 component is the most adequate explanation accounting for the MORB enrichment variability
252 [Staudacher et al., 1989; Dosso et al., 1991; Dosso et al., 1993; Michael et al., 1994; Donnelly
253 et al., 2004; Hémond et al., 2006]. This hypothesis is firstly suggested by the $Na_{8.0}$ variation.
254 $Na_{8.0}$ refers to values of Na_2O corrected from low-pressure fractionation to a common MgO
255 content of 8 wt.% and is considered as an index of the partial meting degree [Klein and
256 Langmuir, 1987]. This parameter is also known to increase with the axial depth, explaining
257 why samples north to the 15°20'N FZ have higher values than those located to the region of
258 the 14°N topographic high previously described (2.8 versus 2.3 in average; Table 1). As
259 proposed by Klein and Langmuir [1987], such depth/chemistry relationship may reflect
260 source heterogeneity in major element composition. The mixing hypothesis is also suggested
261 by the isotope data. The correlations described between our samples isotope ratios indicate
262 that the observed MORB compositional variability probably derived from a binary mixing.
263 Even if the mixing hypothesis was early proposed [Bougault et al., 1988; Staudacher et al.,
264 1989; Dosso et al., 1991; Dosso et al., 1993], the petrological and geochemical processes
265 leading to the formation of enriched sources were not really discussed until recently by
266 Donnelly et al. [2004].

267 These authors underlined that such enrichment requires a low partial melting degree

stage to account for the trace element ratios whereas oceanic ridges are mostly characterized by high melting degrees. To account for the enrichment of a mildly enriched basalt (MARK area), authors have developed a model where the MORB mantle source is contaminated by a metasomatised peridotite, which was previously enriched by low degree partial melts during subduction. Without refuting this model, Hémond et al. [2006] proposed another explanation for E-MORB genesis. Following the observation of McKenzie et al. [2004], they argued that the recycling of alkali basalts composing the great majority of ocean islands and submarine seamounts beneath oceanic ridges could represent an alternative to the metasomatic model proposed by Donnelly et al. [2004]. Both models were developed based on trace element characteristics of E-MORB, and particularly the recurrent occurrence of Nb-Ta positive anomaly. Niu et al. [1999] estimated that Nb-Ta positive anomaly in oceanic basalts indicates that the sources of these basalts are recycled oceanic lithosphere that had previously undergone subduction zone dehydration which preferentially transferred the Th and U (vs. Nb and Ta) to the mantle wedge, leaving a "residual" lithosphere enriched in Nb and Ta. Melting of such enriched lithosphere could therefore enrich the surrounding mantle peridotites and finally produce E-MORB at spreading ridge axis, corroborating the metasomatism model proposed by Donnelly et al. [2004]. Nevertheless, Nb-Ta positive anomaly is also characteristic in overall OIB [e.g. Willbold and Stracke, 2006], probably inherited from the process described by Niu et al. [1999], as recycled oceanic lithosphere is thought to be the major source of OIB [Willbold and Stracke, 2006]. In addition, based on the calculation of trace element variability of the 14°N MAR samples, Hémond et al. [2006] suggested that seamounts can pass through the subduction (in spite of the fractionation related to subduction) without being significantly modified in their trace element composition, even for the more "mobile" element such as Rb and U. Thus, recycling OIB and/or seamounts beneath mid-ocean ridge would also be consistent with the genesis of E-MORB.

293 The main limitation of the latter model is that Hémond et al. [2006] did not extrapolate
294 it to the isotopes. Conversely, Donnelly et al. [2004] used them to demonstrate that the
295 recycling of the oceanic crust cannot explain the isotopic composition of E-MORB, since
296 recycled oceanic crust is expected to have a DMM isotopic composition, which is not
297 radiogenic enough to constitute a suitable source of E-MORB. Based on this assumption, they
298 developed a metasomatic model described above which creates the enrichment necessary to
299 account for the trace element and the isotopic compositions of E-MORB. Similarly to
300 Donnelly et al. [2004], Cooper et al. [2004] considered the origin of Azores E-MORB as
301 related to the melting of a peridotite previously contaminated by melts deriving from the
302 recycling of an old oceanic crust. They suggested that the highly radiogenic Sr composition of
303 E-MORB could be inherited from the hydrothermal alteration of the recycled oceanic crust
304 prior to its subduction. Authors also explain the unradiogenic Nd values by aging effects, but
305 such effects are not only restricted to Nd isotope ratios, and would also affect other isotopic
306 systems. Moreover, this model does not explain the highly radiogenic Pb composition usually
307 observed in E-MORB. Although Pb isotopic compositions can increase due to the seawater
308 alteration, this assumption is far from systematic. Indeed, even Fe-Mn crust contributes to
309 increase Pb isotope ratios [von Blankenburg et al., 1996; Abouchami et al., 1997], Vidal and
310 Clauer [1981] demonstrated that Sr isotopes can show evidences of seawater contamination
311 whereas Pb isotopes do not (this is also the case in this study for some of our samples, Figure
312 3). The major argument against Donnelly et al.'s model [2004] [and also the one of Cooper et
313 al., 2004] concerns the depth of the first melting stage. In both models, low F melting of the
314 subducting slab is believed to occur at greater depths than those usually considered for arc-
315 magma genesis [i.e. ~110 km; e.g. Hattori and Guillot, 2003; Rüpke et al., 2004]. This
316 assumption may be problematic for two reasons: Firstly, melting of subducting slab requires
317 particular conditions that are far from systematic in subduction zones. Iwamori [1998]

demonstrates that slab melting is restricted to young slab (<10 My), mainly producing particular arc-magmas such as adakites. Such melting generally occurs in the forearc and is thus localized at low depth [<80 km; Iwamori, 1998]. Secondly, melting is unlikely to occur at depths greater than ~150 km. Melting in subduction is associated to the breakoff of hydrous minerals (i.e. serpentine) composing the slab and/or the overlying mantle wedge that release an important amount of water leading to its partial melting [e.g. Hattori and Guillot, 2003; Rüpke et al., 2004]. Even small amount of water can be retained in the slab at depth greater than 150 km, the pressure is likely too high and the amount of water too low to produce slab-derived melts. Therefore, while these observations are not sufficient to rule out the metasomatism model of Donnelly et al. [2004], they allow us to consider further the OIB recycling model of Hémond et al. [2006]. Nevertheless, to validate the model of Hémond et al. [2006], isotopic compositions must be taken into account, particularly considering that even if OIB can be estimated as homogeneous in trace element composition, this assumption is not true for isotopes.

5.2 OIB recycling model.

5.2.1 Formation of seamounts: On-axis vs. off-axis origin.

The major feature that has to be taken into account before considering the model of seamount recycling is the origin of the seamounts. Indeed, the viability of the model critically depends on how do the seamounts form and do all of them display enriched composition that could contribute to produce E-MORB after their recycling. Basically, seamounts can be related to: (1) a hotspot activity; (2) a mid-ocean ridge activity; (3) a intra-oceanic subduction zone. Although seamounts deriving from arc magmatism are clearly different in composition compared to the DMM, their number is very limited [Koppers and Watts, 2010] and thus their contribution to the mantle heterogeneity can be considered as negligible.

Volcanic islands and seamounts formed away from tectonic boundaries (so-called intra-plate volcanism, e.g. Hawaii-Emperor chain, Society Islands, Réunion, Cape Verde) are commonly considered as the surface expression of deep mantle plume activity [Morgan, 1971]. In this "off-ridge" setting [Watts et al., 2006; Koppers and Watts, 2010], such intra-plate magmatism leads to the formation of large volcanic islands (locating the present-day hotspot activity) which become seamounts as the plate motions move them away from the "stationary" parent plume, forming linear age-progressive seamount trails. Basalts related to hotspots (so-called OIB for oceanic island basalts) differ from MORB in their chemical composition. Unlike the MORB, which are tholeiites thought to be formed by high degrees of partial melting (>10%), OIB are mainly silica-undersaturated alkali basalts deriving from low degrees of partial melting and which are enriched in incompatible elements and radiogenic isotope ratios relative to MORB [e.g. Hofmann et al., 1978; Zindler and Hart, 1986]. As they were believed to derive from a deep source [i.e. the D" layer at the Core-Mantle boundary; Morgan, 1971], OIB offered a unique opportunity to understand deep mantle processes. Therefore numerous studies focused on them over the last three decades [e.g. Hofmann et al., 1978, White, 1985; Zindler and Hart, 1986; Hart et al., 1992; Stracke et al., 2005; Willbold and Stracke, 2006; 2010]. These studies have demonstrated that OIB do not derive from a unique source and that they arise from the mixing of approximately five mantle reservoirs (DMM, EM-1, EM-2, HIMU and FOZO/PREMA/PHEM/C) defined by their isotope ratios [Zindler and Hart, 1986], leading to a scheme nicknamed "the mantle zoo" [Stracke et al., 2005]. Compared with the DMM, presumed to approximate the source of the MORB, EM-1 (Enriched-Mantle-1) is characterized by high $^{87}Sr/^{86}Sr$, very low $^{144}Nd/^{143}Nd$ and higher $^{208}Pb/^{206}Pb$ at a given $^{206}Pb/^{204}Pb$, properties that are thought to be inherited from the recycling of pelagic sediments in the source of magmas. OIB that fall into this category are Pitcairn, Kerguelen, Walvis Ridge, Tristan da Cunha and Gough. OIB from EM-2 source (Enriched-

368 Mantle-2) are more radiogenic in Sr and Pb and less radiogenic in Nd than EM-1 and are
369 associated to the recycling of terrigenous sediments eroded from the continental crust and
370 deposited on the seafloor. Society, Samoa and Marquesas Islands are representative of EM-2
371 type OIB. HIMU (for HIgh μ, i.e. high $^{238}U/^{204}Pb$) type OIB includes St Helena and some of the
372 Cook-Austral chain basalts (others belong to the FOZO type, see below) and are characterized
373 by extremely high Pb isotope ratios. They are also less radiogenic in Sr compared to EM-
374 types and are likely to be formed by the recycling of old, subducted, dehydrated oceanic crust.
375 Compared to HIMU, the last classification, called FOZO [for FOcal ZOne, Hart et al., 1992;
376 Stracke et al., 2005] was attributed to OIB that were less radiogenic in Pb at a given Sr and
377 Nd isotopic composition. FOZO is mainly represented in basalts from Cook-Austral chain
378 [see Stracke et al., 2005], and it is also considered to be common to most basalts. The idea of
379 a common component mixed in the various sources of OIB, first called PREMA [for
380 PREvalent MAntle, Zindler and Hart, 1986], has evolved to FOZO, PHEM [for Primitive
381 HElium Mantle, Farley et al., 1992] and C [Common Component, Hanan and Graham, 1996],
382 but all of them differ from each other only in detail [Hofmann, 2003]. As the name and the
383 origin of this component have no influence on the proposed model, we will simply refer to
384 FOZO hereafter.

385 As their chemistry strongly differs from the DMM, the recycling of OIB may introduce
386 significant amount of enriched material in the mantle. Nevertheless, intraplate oceanic
387 seamounts do not all originate from plumes. Even, several studies have shown that this type
388 of seamount is predominant in the seafloor compared to OIB related seamounts [Batiza, 1982;
389 Hofmann, 1997; Watts et al., 2006; Koppers and Watts, 2010]. They usually occur as isolated
390 edifices (near-ridge seamounts, e.g. along the EPR), clusters (Rano-Rahi seamount field, near
391 the EPR) or lines (the Cameroon Line in the Atlantic ocean or the Line Islands and the
392 Pukapuka ridge in the Pacific Plate). As only few data are available on this type of seamounts,

393 their origin remains poorly constrained, Hofmann [1997] arguing that most of these are
394 melting anomalies likely coming from the upper mantle. Following this idea, the hypothesis
395 of small-scale sublithospheric convection [Ballmer et al., 2007] has been developed to explain
396 linear seamount chains that do not display age progression (such as Pukapuka ridge or Line
397 Islands) or seamount clusters (Rano-Rahi seamount field). Recently, on the basis of the elastic
398 thickness, a parameter that is sensitive to whether a seamount is formed nearby of faraway
399 from a mid-ocean ridge, Watts et al. [2006] and Koppers and Watts [2010] estimated that the
400 largest part of the world's seamounts are not related to plume and was formed close to mid-
401 ocean ridge (i.e. "on-ridge" type seamount). Studies focused on these "on-ridge" seamounts
402 have shown that they are geochemically different from N-MORB, carrying slightly enriched
403 MORB-like signatures [Batiza and Vanko, 1984; Zindler et al., 1984; Graham et al., 1988;
404 Niu et al., 1997; 2002]. In reality, non-OIB seamounts display large variations in composition,
405 ranging from N-MORB-like signature to OIB-like signatures (Fig. 4). Particularly, numerous
406 EPR seamounts have isotopic compositions that are highly comparable with those assumed
407 for the DMM. However, most of the "on-ridge" seamounts exhibit slightly to strongly
408 enriched compositions and plot along the DMM-FOZO array. This indicates that such type of
409 seamounts derives from the mixing of small-scale heterogeneities with the surrounding
410 depleted upper mantle and thus also incorporates a significant amount of enriched material in
411 the mantle when they are recycled.
412 Nevertheless, although we show that "on-ridge" type seamounts are slightly enriched
413 compared to the DMM, both types of seamounts do not have the same potential to produce E-
414 MORB after their recycling. As illustrated above, "on-ridge" seamounts differ from "off-
415 ridge" seamounts mainly on their number, their size and their chemistry. Hillier and Watts
416 [2007] estimate a total number of ~3 million seamounts with a height > 0.1 km of which only
417 200,000 are clearly identified. Considering these numbers, only a few of them are clearly

418 documented enough to constrain their origin. However, Watts et al. [2006] and Koppers and
419 Watts [2010] recently estimated that at least 60% of the identified seamounts were formed in
420 an "on-ridge" setting (estimate made using the Wessel's [2001] database of ~15,000
421 seamounts with a height >1.5 km). Although "off-ridge" seamounts are less abundant, they
422 are significantly more enriched in incompatible elements and more radiogenic in Sr and Pb
423 isotopes. Among all "on-ridge" seamounts plotted in Figure 4, only a few reaches the
424 radiogenic enrichment usually described in OIB (e.g. the Cameroon line or some samples
425 from the Line Islands). All others more closely resemble E-MORB rather than OIB. "Off-
426 ridge" seamounts are also higher in size and volume [Batiza, 1982; Wessel, 2001]. For
427 instance, the almost totality of the structures that form the Hawaiian-Emperor seamount
428 chains are higher than 4 km, while "on-ridge" seamounts are smaller (likely < 1.5 km in
429 average) suggesting that the largest amount of enriched material that derives from the
430 recycling of seamounts is related to OIB.
431
432 *5.2.2 Trace element modeling.*
433 The trace element modeling reproduced in this study is nearly the same as developed in
434 Hémond et al. [2006]. This model was used to constrain the Sr, Nd and Pb concentrations in
435 the enriched component, data that are required for isotope modeling. Parameters used in this
436 model and their references are given in Table 2 and 3 (see also Table S1 for complete
437 parameter values used for the modeling including partition coefficients, average compositions
438 in trace elements and isotopes for OIB, etc.).
439 The assumption of Hémond et al.'s modeling is that E-MORB from the 14°N anomaly
440 in the MAR derive from the melting of an enriched source which can be modeled as a solid
441 binary mixing process between the DMM and enriched component (i.e. a recycled
442 OIB/seamount). For purpose of modeling, the trace element composition of the recycled

OIB/seamount is calculated using the non-modal batch meting equation from Shaw [1970] and the solid binary mixing model developed by Faure [1977]. The non-modal batch melting equation defined by Shaw [1970] is turned to express the trace element concentration of the E-MORB source (C_0) as a function of the trace element composition of the E-MORB (C_{EL}), the partial melting degree (F), the source bulk distribution coefficient (D_0) and the melt partition coefficient (P):

$$C_0 = \frac{C_{EL}}{D_0 + F(1-P)} \quad (1)$$

The most enriched E-MORB (sample 428R5) was chosen for the melt composition (C_{EL}). It makes sense to use this sample in this purpose as this sample comes from the area where the contamination by the enriched component is the strongest. As postulated by Hémond et al. [2006], a relatively high partial melting degree (F = 18 %) was used because of the enhanced fertility caused by the addition of the enriched component within the DMM.

The same expression as (1) is used to constrain the trace element composition of the N-MORB source (i.e. the DMM):

$$C_{DMM} = \frac{C_{N-MORB}}{D_0 + F(1-P)} \quad (2)$$

Here, C_{DMM} is the trace element composition of the DMM and $C_{N\text{-}MORB}$ corresponds to an average of N-MORB trace element composition (N-MORB are here defined as MORB with $(La/Sm)_N < 1$ and $^{87}Sr/^{86}Sr < 0.7027$). D_0 and P are the same as in (1) and F = 10 %, following the model of Hémond et al. [2006]. Then, the composition of the enriched component (i.e. the recycled OIB/seamount; C_{EC}) drowned in the surrounding, more depleted, mantle source (i.e. the DMM; C_{DMM}) is deduced from the solid binary mixing equation given in Faure [1977]:

$$C_0 = C_{EC}.f + C_{DMM}.(1-f) \quad (3)$$

turned into

$$C_{EC} = \frac{C_0 - C_{DMM}.(1-f)}{f} \quad (4)$$

where f corresponds to the proportion of the enriched component in the mixture.

In Figure 5, the trace element spidergrams of two calculated enriched components (red lines) are reported and compared with the OIB fields [Willbold and Stracke, 2006]. The "0.05:1" and "0.15:1" lines represent the PM-normalized trace element compositions of the modeled recycled OIB/seamount calculated for f = 5 % and 15 %, respectively (see Table 3 for the compositions). Contrary to Hémond et al. [2006] who chose the abundance patterns of the recycled OIB/seamount "so that the final model product matches the observed, average E-MORB at 14-15°N exactly", we calculate here the trace element composition of the enriched component at different mixing proportions with respect to the OIB fields. In other words, we consider in our calculation that the modeled enriched component is consistent with "natural" OIB when at least 90% of the PM-normalized values plot within OIB field. Even if mixing proportions were chosen to stay within the OIB field, Figure 5 demonstrates that chondrite-normalized trace element patterns are consistent with "natural" OIB composition (i.e. incompatible element enrichment, positive Nb-Ta anomaly, HREE depletion). Furthermore, these mixing proportions (5 to 15 %) are closed to the abundance of recycled material present in north Atlantic MORB source [≤10%, Cooper et al., 2004]. Our estimates can be closer (6 to 11 %) to those of Cooper et al. [2004] by considering only modeled patterns of which 100% of the chondrite-normalized values plot within OIB field.

5.2.3 Isotope modeling.

Isotope ratios of the enriched component were calculated using the binary mixing equation developed by Faure [1977] and DePaolo and Wasserburg [1979]:

$$IC_m = \frac{fC_{EC}IC_{EC} + (1-f)C_{DMM}IC_{DMM}}{fC_{EC} + (1-f)C_{DMM}} \quad (5)$$

where IC_m, IC_{EC} and IC_{DMM} are respectively the isotopic compositions of the mixture, the enriched component and the DMM, C_{EC} and C_{DMM} are the elemental concentrations in both components and f is the proportion of the enriched component in the mixture. Results of trace element modeling were used for Sr, Nd and Pb concentrations, as well as the mixing proportions. Isotope ratios of the mixture and the DMM were determined by the same way as for the trace elements: isotope ratios of the most enriched E-MORB (sample 428R5) were chosen as ratios of the mixture, and DMM isotope ratios correspond to the regional average of N-MORB isotope ratios. Other parameters are summarized in Table 2 and Table S2. Results are presented in Figure 6 and Table 3.

Contrary to the results given by the trace element modeling, variations in the mixing proportions do not lead to significant changes in the modeled enriched component composition. The modeling results are ~0.70292 for $^{87}Sr/^{86}Sr$, ~0.51287 for $^{143}Nd/^{144}Nd$ ratio, ~19.564 for $^{206}Pb/^{204}Pb$ ratio, ~15.594 for $^{207}Pb/^{204}Pb$ ratio and 39.22 for $^{208}Pb/^{204}Pb$ ratio. Compared to OIB fields, the calculated enriched component appears incompatible with both EM endmembers. Sr and Nd isotopes are consistent with HIMU, but Pb isotopes are too low to fit with the extremely radiogenic values characterizing HIMU. However, all isotope ratios are comparable with the FOZO isotope compositions, which are characterized by lower Pb isotopic composition at given Sr and Nd. Considering that both trace element and isotope modelings reach the same results, the recycling of OIB seems to be a reasonable model to explain the E-MORB genesis at 14°N on the MAR.

5.3 Does this happen somewhere else ?

Although our model can explain the MORB enrichment in the 14°N region in the MAR, its validity at a global scale (whether this model can account for MORB enrichment in other ridge environment or not) has to be verified. To test this hypothesis, we used samples from

515 the Central Indian Ridge (CIR) at 18°S [Nauret et al., 2006], as in many points, they resemble
516 to the samples from the 14°N anomaly in the MAR: (1) Samples are enriched in incompatible
517 elements ($(La/Sm)_N$ >1), (2) they display Nb-Ta positive anomaly, (3) they are highly
518 radiogenic in Sr and Pb and isotopically depleted in Nd compared to the DMM.

519 Nauret et al. [2006] suggested that "the CIR MORB, between 18° and 20°S are
520 generated by partial melting of a heterogeneous source consisting of an enriched component
521 and a normal, depleted upper-mantle peridotite". These authors also highlighted that "the
522 nature of the enriched component is a matter of speculation". They finally noticed that this
523 enrichment is not related to the presence of a hotspot, as the E-MORB composition is distinct
524 from the Réunion plume composition, which is the closest hotspot in the area. Instead, Nauret
525 et al. [2006] considered that the enriched component could result from the metasomatic event
526 proposed by Donnelly et al. [2004], even if enrichment by recycling ancient alkali basalt is
527 also considered.

528 The model established on trace elements and isotopes for the samples from the 14°N
529 region in the MAR was extrapolated to the 18°-20°S region of the CIR. Calculations were
530 made using sample GNT-Pl1-1 since it corresponds to the most enriched sample. Results are
531 presented in Figure 7 and Table 3 (all plots are available in supplementary Figure S1). Trace
532 element composition of the calculated enriched component is comparable to OIB
533 compositions using mixing proportions varying between 1 % and 5 %. Applying these results
534 on the isotope modeling gives an enriched component more radiogenic in Sr (~ 0.70525), less
535 radiogenic in Nd and ^{206}Pb (~ 0.51270 and ~ 18.955 respectively) and almost identical in
536 $^{207}Pb/^{204}Pb$ and $^{208}Pb/^{204}Pb$ (~ 15.618 and ~ 39.19) compared to the one calculated for the 14°N
537 anomaly in the MAR. As illustrated in Figure 7, this enriched component is consistent with
538 common EM 2 basalts, demonstrating that the model of OIB recycling can also explain
539 MORB enrichment in this region.

More generally, several studies reported the existence of E-MORB along mid-ocean ridges of which at least a part presents identical geochemical characteristics (incompatible element enrichment, Nb-Ta positive anomaly, isotopically enriched in Sr and Pb, depleted in Nd) to E-MORB from 14°N in the MAR. This is the case, for example, of MORB sampled along the MAR at 23°N [Donnelly et al., 2004] and 33°S [Michael et al., 1994], as well as for those located at 11°20'N along the EPR [Niu et al., 1999]. Although our model was not tested in these cases due to incomplete data set, the existence of these MORB with geochemical characteristics as listed above (particularly the Nb-Ta positive anomaly) allows us to suppose that our modeling is expected to work on these regions too.

Finally, we notice that the mixing proportions determined from the CIR samples are notably the same as those calculated for the 14°N anomaly (globally < 10 %). This result is compatible with previous results obtained by Cooper et al. [2004] who estimated that the materials responsible for the genesis of E-MORB in the North Atlantic are present in abundances of 2-5 % in average. However, these abundances are used by Cooper et al. to explain the pollution of upper mantle at a global scale while ours explain smaller heterogeneities along mid-ocean ridges. This means that the percentage of the recycled OIB/seamount in the mantle source of MORB could be greater if required without being in opposition to the model of Cooper et al. [2004; 2009]. In any case, the small amount we calculated together with the generally small scale heterogeneity that represent E-MORB we studied along the MAR and the CIR suggest that the enriched component represents a very small volume (maybe a few cubic kilometer scale) drowned in the surrounding "normal" mantle. This statement is compatible with the recycling of OIB or seamount which are below the sea level and thus small sized when they subduct.

5.4. Hyperbolic *versus* straight mixing trends.

As developed by Langmuir et al. [1978], mixing relationships in isotope spaces form linear or hyperbolic trends depending on the denominators in the isotope ratios and on the elemental ratio of both mixing components: if the denominators in isotope ratios are identical (as in the lead isotopes, i.e. ^{204}Pb), the mixing trend is a straight line. Else, the mixing trend depends on the ratio of elemental concentrations in both mixing components:

$$K = \frac{(C_x^a / C_y^a)}{(C_x^b / C_y^b)} \quad (6)$$

Choosing for example Sr for *x* and Nd for *y,* it becomes

$$K = \frac{(Sr / Nd)_a}{(Sr / Nd)_b} \quad (7)$$

in which *a* and *b* are the mixing endmembers. If K=1, the mixing trend is also a straight line. Else, it is an hyperbola. In Figure 6 and 7, plotting the model results with the data shows essentially straight lines, even in Nd-Sr, Sr-Pb and Nd-Pb isotopic projections where hyperbolic trends are likely to occur. As described above, this feature can be explained by a K value of ~1, showing that the ratios of elements (i.e. Sr/Nd, Sr/Pb and Nd/Pb) are approximately the same in both end-members. This seems to be paradoxical, since our model involves a mixing between the DMM and an enriched OIB source. Figure 8 presents histograms showing the frequency and variation of element ratios (Sr/Nd, Sr/Pb and Nd/Pb) in MORB and OIB. This figure illustrates the broad overlap in the range of Sr/Nd, Sr/Pb and Nd/Pb ratios in MORB and OIB. We found average ratios of 12.8, 247 and 20.1 for Sr/Nd, Sr/Pb and Nd/Pb ratios in MORB, respectively. Average ratios calculated for the OIB approximate those of MORB, leading to K values closed to 1 (calculated here as the ratios in MORB divided by those in OIB). As an example, a virtual mixing between sediments and the DMM leads to a K that can be higher than 20 [calculated using the Nd/Pb ratios of the GLOSS from Plank and Langmuir, 1998]. Therefore, as element ratios in MORB and in OIB are similar, a mixing between these two components will form curvilinear trends rather than

589 hyperbolas in isotope spaces.

590

591 **5.5 Time constraints.**

592 Several studies try to constrain the age of the heterogeneities responsible for E-MORB
593 genesis [e.g. Dosso et al., 1999; Cooper et al., 2004; Donnelly et al., 2004]. Using mantle
594 isochrons and Monte-Carlo simulations on Sr, Nd and Pb isotope systems, Dosso et al. [1999]
595 give an age of 250 Ma for the heterogeneity beneath the 14°N region. The same age is also
596 given for the enriched component beneath the Azores [Dosso et al., 1999; Cooper et al., 2004].
597 Cooper et al. [2004] extrapolate this age to all enriched components present in the North-
598 Atlantic MORB source (excluding deep hotspot), arguing that all of them represent recycled
599 products subducted along the western margin of Pangea. In their study, Donnelly et al. [2004]
600 also calculated an age of ~300 Ma based on mantle isochrons, but also showed that this age
601 does not necessarily represent a specific event. Instead, they assume that this age results from
602 the continuous formation and destruction of the enriched mantle source and depends on
603 multiple parameters such as the decay constant of the radioactive decay system or the
604 incompatibility of the daughter element during melting. They finally demonstrated that the
605 mantle isochron ages could approximate the residence time of the enriched reservoir in the
606 mantle if its mass represents a few percent of the system.

607 Figure 9 shows the evolution of the $^{206}Pb/^{204}Pb$ and $^{208}Pb/^{204}Pb$ compositions with the time,
608 calculated for both modeled recycled OIB/seamount (14°N in the MAR and 18°-20°S region
609 of the CIR) and compared to the evolution of the DMM. Considering that the Pb isotopic
610 composition of the recycled OIB/seamount cannot be more depleted than the DMM, a
611 maximum age is given by the intersection between both evolution lines. Pb isotope systems
612 give apparent ages ranging from 266 Ma to 295 Ma for the recycled OIB/seamount beneath
613 the 14°N anomaly in the MAR, which is closed to the ~ 250 Ma estimated by Dosso et al.

614 [1999] and Cooper et al. [2004]. Age calculated for the recycled OIB/seamount in the CIR
615 region ranges from 298 Ma to 332 Ma. Using extremely depleted isotopic compositions for
616 the DMM (D-DMM in Figure 9), ages measured for recycling OIB in both regions are ~ 400-
617 550 Ma. Tackley [2000] demonstrated that the time scale of complete mantle overturn (i.e.
618 travel down to core-mantle boundary and back to surface) approximates 400-500 Myr. This
619 suggests that recycling OIB underwent a maximum of one "cycle" within the mantle before
620 reappearing beneath the ridge. Considering that the 400-500 Myr age is obtained for an
621 extremely (anomalously) depleted mantle composition, an age of ~250 Ma seems more
622 reasonable, suggesting that the recycled OIB/seamount likely never entered the deep mantle
623 (Fig. 10).
624
625 **5.6 Reconciling the OIB/seamount recycling model and the oxygen isotope**
626 **composition of MORB**
627 Recently, Cooper et al. [2009] have published a compilation of available laser
628 fluorination $\delta^{18}O$ data for MORB form the Atlantic, Indian and Pacific ridges and have used it
629 to constrain the nature and percentage of enriched material within the upper mantle globally.
630 They revealed that the $\delta^{18}O$ compositions of MORB from each ocean basin fit a normal
631 distribution, with identical means and standard deviations ($\delta^{18}O_{mean}$ ~5.50 ‰) and with a total
632 range of 5.25 - 5.8%. In addition, they showed that the oxygen isotope data correlate with
633 radiogenic isotope and trace element. Based on this, Cooper et al. [2009] suggested the DMM
634 to have a $\delta^{18}O$ composition of ~5.25 ‰ and the average measured value of 5.5 ‰ to reflect a
635 global contamination of the upper mantle by recycling crustal material in proportion ranging
636 from 5 to 10% (taking into account that these estimates may vary depending on the
637 sedimentary contents in the recycled material). This model is much in favor of the Donnelly et
638 al.'s model rather than ours, since ones can assume that the OIB/seamount recycling model

cannot account for the apparent correlation between oxygen isotope data and radiogenic isotope or trace element, because OIBs display the same range in $\delta^{18}O$ composition as MORB [Eiler et al., 1996; Eiler, 2001]. Eiler et al. [1996] have reported the $\delta^{18}O$ composition of olivine from basalts belonging to each subtype of OIB (i.e. HIMU, EM 1, EM 2 and others including some of the FOZO group). Their results show no evidence for $\delta^{18}O$ values outside the range for MORB, except for EM 2 type OIB, of which anomalously high $\delta^{18}O$ compositions reflect the presence of subducted sediments in their mantle source.

Therefore, taking into account the results of Cooper et al. [2009], trends in $\delta^{18}O$ plotted versus trace elements or isotope data are not consistent with the OIB/seamount recycling model unless the OIB that are recycled are all EM 2. However, this assessment can be addressed by at least two reasons: Firstly, although $\delta^{18}O$ data are clearly of a certain interest in the study of mantle heterogeneities, the correlations proposed by Cooper et al. [2009] are not always well defined (this is particularly true for Pacific samples which exhibit a large range of $\delta^{18}O$ compositions at a given Sr and Pb isotopic composition). Although the weakness of the correlations may be related to the lack of high resolution oxygen data such as those published by Cooper et al. [2004; 2009], these correlations have to be considered with caution and are not robust enough to rule out the OIB/seamount recycling model. Moreover, as oxygen isotope data are available neither in the 14°N region of the MAR nor in the 18-20°S of the CIR, there is no evidence for a possible application of the Copper et al.'s model in these regions. That is not ruling out the model of Cooper et al. [2009], but without a denser database in oxygen isotopes for MORB, one could admit that correlations may occur at large scale (ocean scale) while they do not at more restricted scale (not more than few hundred kilometers). Secondly, the model defended by Cooper et al. [2009] is not incompatible with ours as both could actually happen synchronously in different localities, i.e. a recycled seamount could represent the enriched material in some areas while other types of enriched

materials could contribute to form E-MORB in others. The main difference between the two models resides in that the recycling of the oceanic crust may account for large scale heterogeneities (e.g. the global enrichment in oxygen isotopes of the upper mantle at ocean scale, as postulated by Cooper et al., 2009] while the recycling of OIB/seamounts are more likely to form very restricted MORB enrichments (no more than hundred kilometers).

5.7 Recycled seamounts: more than a process for local MORB enrichment ?

We show in this paper that recycling OIB can be a viable process to explain the genesis of E-MORB at 14°N in the MAR, but it is also susceptible to explain E-MORB genesis along other ridges. As demonstrated above, E-MORB from the 18°S region of the CIR, and in regions potentially presenting similar geochemical features (MORB at 23°N and 33°S in the MAR and those from 11°20'N in the EPR) could be explained by this process. This suggests that the recycling of OIB is not an isolated process. Wessel [2001] and Hillier and Watts [2007] identified slightly less than 15,000 seamounts with a heigh >1.5 km, and almost a half of them resides on the Pacific plate. Although the size of a seamount is negligible compared to the volume of the mantle, calculations made by Hillier and Watts [2007] show that overall identified seamounts cover more than 18% of the oceanic seafloor area. A virtual addition of these numerous seamounts allows a thickening of the oceanic crust of about 180 m. Considering these estimates and those of Hofmann [1997] which showed that 20 km^3 of oceanic crust are recycled per year, we can calculate that seamounts represent approximately 2% of the recycled material. Taking into account that the values given by Hillier and Watts [2007] are minima estimates, i.e. using only identified and measured edifices and that the authors expect around 3 millions of seamounts with a height >0.1 km, the proportion of seamounts in the recycled material can significantly increase. Thus, considering the trace element budget, the isotopic composition of the mantle and the 5-10 % estimation for the total

689 recycled material in the upper mantle with seamounts representing ~2 %, it is clear that the
690 recycling of seamount can hardly be considered as a significant contributor to the upper
691 mantle heterogeneity. Nevertheless, it has to be considered as a plausible mechanism to
692 generate (local) MORB enrichment.
693
694 **CONCLUSIONS.**
695 New trace element and isotope data have demonstrated that MORB enrichment from
696 north and south of the 15°20'N FZ can find their origin in the geochemical anomaly centered
697 at 14°N and associated with a high topographic bulge.
698 Isotope ratios confirm and valid the enrichment model established on trace element by
699 Hémond et al. [2006]: the E-MORB origin can be attributed to a binary mixing between N-
700 MORB source and OIB/seamount material recycled through subduction. The age of the
701 recycled OIB/seamount is estimated to 250 Ma.
702 Finally, we show that the model described here can be applied to E-MORB from other
703 ridge segments, and is thus unlikely to be an isolated process. Considering the great number
704 of seamounts on the ocean floor, their recycling may represent a significant process to
705 account for MORB enrichment.
706
707 **Acknowledgements.**
708 M.U., C.H. and P.N. thank Claire Bollinger and Marcel Bohn for their help during the laboratory and analytical
709 works, and Philippe Telouk for his help during lead isotope measurements at the ENS of Lyon. We also thank
710 Catherine Chauvel, Al Hofmann, Charlotte Fillon and Morgane Ledevin for their help during the redaction of the
711 manuscript.
712 K.P.J. thanks Brigitte Stoll for its contribution during trace element measurements at the Max-Plank-Institut für
713 Chemie of Mainz.
714 We also thank the editor Joe Baker and the two anonymous reviewers and Matthew Jackson for their comments
715 that help us to significantly improve this manuscript.

716 **References.**

717 Abouchami W., Goldstein, S.L., Gazer, S.J.G., Eisenhauer, A., and Mangini, A., 1997.
718 Secular changes of lead and neodymium in central Pacific seawater recorded by a Fe-
719 Mn crust. Geochimica et Cosmochimica Acta, 61(18): 3957-3974.

720 Abouchami, W., Galer, S.J.G. and Hofmann, A.W., 2000. High precision lead isotope
721 systematics of lavas from the Hawaiian Scientific Drilling Project. Chemical Geology,
722 169(1-2): 187-209.

723 Agranier, A. Blichert-Toft, J., Graham, D., Debaille, V., Schiano, P., and Albarède, F., 2005.
724 The spectra of isotopic heterogeneities along the mid-Atlantic Ridge. Earth and
725 Planetary Science Letters, 238(1-2): 96-109.

726 Allègre, C.J., Hamelin, B. and Dupré, B., 1984. Statistical analysis of isotopic ratios in
727 MORB - The Mantle Blob Cluster model and the convection regime of the mantle.
728 Earth and Planetary Science Letters, 71(1): 71-84.

729 Arevalo, R. Jr, and McDonough, W.F., 2009. Chemical variations and regional diversity
730 observed in MORB. Chemical Geology, 271: 70-85.

731 Blichert-Toft, J., Weis, D., Maerschalk, C., Agranier, A. and Albarède, F., 2003. Hawaiian
732 hot spot dynamics as inferred from the Hf and Pb isotope evolution of Mauna Kea
733 volcano. Geochemistry Geophysics Geosystems, 4: doi:10.1029/2002GC000340.

734 Ballmer, M.D., van Hunen, J., Ito, G., Tackley, P.J., Bianco, T.A., 2007. Non-hotspot volcano
735 chains originating from small-scale sublithospheric convection. Geophysical Research
736 Letters, 34: L23310.

737 Batiza, R., 1982. Abundances, distribution and sizes of volcanoes in the Pacific Ocean and
738 implications for the origin of non-hotspot volcanoes. Earth and Planetary Science
739 Letters, 60: 195–206.

740 Batiza, R., Vanko, D., 1984. Petrology of young Pacific seamounts. Journal of the

741 Geophysical Research, 89: 11,235–11,260.
742 Bonatti, E., Peyve, A., Kepezhinskas, P., Kurentsova, N., Seyler, M., Skolotnev, S., Udintsev,
743 G., 1992. Upper mantle heterogeneity below the Mid-Atlantic Ridge, 0° to 15°N.
744 Journal of Geophysical Research-Solid Earth, 97(B4): 4461-4476.
745 Bougault, H., Dmitriev, L., Schilling, J.G., Sobolev, A., Joron, J.L., Needham, H.D., 1988.
746 Mantle heterogeneity from trace elements: MAR triple junction near 14°N. Earth and
747 Planetary Science Letters, 88(1-2): 27-36.
748 Cannat, M., Bideau, D. and Bougault, H., 1992. Serpentinized peridotites and gabbros in the
749 Mid-Atlantic Ridge axial valley at 15°37'N and 16°52'N. Earth and Planetary Science
750 Letters, 109(1-2): 87-106.
751 Cannat, M., Lagabrielle, Y., Bougault, H., Casey, J., de Coutures, N., Dmitriev, L., and
752 Fouquet, Y., 1997. Ultramafic and gabbroic exposures at the Mid-Atlantic Ridge:
753 geological mapping in the 15°N region. Tectonophysics, 279(1-4): 193-213.
754 Castillo, P.R., Klein, E., Bender, J., Langmuir, C., Shirey, S., Batiza, R., and White, W., 2000.
755 Petrology and Sr, Nd, and Pb isotope geochemistry of mid-ocean ridge basalt glasses
756 from the 11°45′N to 15°00′N segment of the East Pacific Rise. Geochemistry
757 Geophysics Geosystems, 1: doi:10.1029/1999GC000024.
758 Castillo, P.R., Natland, J.H., Niu, Y.L. and Lonsdale, P.F., 1998. Sr, Nd and Pb isotopic
759 variation along the Pacific-Antarctic risecrest, 53-57°S: Implications for the
760 composition and dynamics of the South Pacific upper mantle. Earth and Planetary
761 Science Letters, 154(1-4): 109-125.
762 Charlou, J.L., Bougault, H., Appriou, P., Nelsen, T. and Rona, P., 1991. Different TDM/CH 4
763 hydrothermal plume signatures: TAG site at 26°N and serpentinized ultrabasic diapir at
764 15°05'N on the Mid-Atlantic Ridge. Geochimica et Cosmochimica Acta, 55(11): 3209-
765 3222.

766 Cooper, K.M., Eiler, J.M., Asimow, P.D., Langmuir, C.H., 2004. Oxygen isotope evidence
767 for the origin of enriched mantle beneath the mid-Atlantic ridge. Earth and Planetary
768 Sciences Letters, 220(3-4): 297-316.
769 Cooper, K.M., Eiler, J.M., Sims, K.W.W., Langmuir, C.H., 2009. Distribution of recycled
770 crust within the upper mantle: Insights from the oxygen isotope composition of MORB
771 from the Australian-Antarctic Discordance. Geochemistry Geophysics Geosystems 10:
772 doi:10.1029/2009GC002728.
773 Cousens, B.L., Allan, J.F., Leybourne, M.I., Chase, R.L. and Vanwagoner, N., 1995. Mixing
774 of magmas from enriched and depleted mantle sources: the northeast Pacific - West
775 Valley segment, Juan de Fuca Ridge. Contributions to Mineralogy and Petrology,
776 120(3-4): 337-357.
777 DePaolo D.J. and Wasserburg, G.J., 1979. Petrogenetic mixing models and Nd-Sr isotopic
778 patterns. Geochimica et Cosmochimica Acta, 43: 615-627.
779 Donnelly, K.E., Goldstein, S.L., Langmuir, C.H. and Spiegelman, M., 2004. Origin of
780 enriched ocean ridge basalts and implications for mantle dynamics. Earth and Planetary
781 Science Letters, 226(3-4): 347-366.
782 Dosso, L., Bougault, H. and Joron, J.-L., 1993. Geochemical morphology of the North Mid-
783 Atlantic Ridge, 10°-24°N: Trace element-isotope complementarity. Earth and Planetary
784 Science Letters, 120(3-4): 443-462.
785 Dosso, L., Hanan, B.B., Bougault, H., Schilling, J.-G. and Joron, J.-L., 1991. Sr-Nd-Pb
786 geochemical morphology between 10° and 17°N on the Mid-Atlantic Ridge: A new
787 MORB isotope signature. Earth and Planetary Science Letters, 106(1-4): 29-43.
788 Dupré, B. and Allègre, C.J., 1983. Pb-Sr isotope variation in Indian Ocean basalts and mixing
789 phenomena. Nature, 303(5913): 142-146.
790 Eiler, J.M., Farley, K.A., Valley, J.W., Hofmann, A.W., Stolper, E.M., 1996. Oxygen isotope

791 constraints on the sources of Hawaiian volcanism. Earth and Planetary Science Letters,
792 144: 453–467.
793 Eiler, J.M., 2001. Oxygen isotope variations of basaltic lavas and upper mantle rocks.
794 Reviews of Mineralogy and Geochemistry, 43, 319–364.
795 Eisele, J.R., Abouchami, W., Galer, S.J.G. and Hofmann, A.W., 2003. The 320 kyr Pb isotope
796 evolution of Mauna Kea lavas recorded in the HSDP-2 drill core. Geochemistry
797 Geophysics Geosystems, 4: doi:10.1029/2002GC000339.
798 Escartin, J. and Cannat, M., 1999. Ultramafic exposures and the gravity signature of the
799 lithosphere near the Fifteen-Twenty Fracture Zone (Mid-Atlantic Ridge, 14 °-16.5°N).
800 Earth and Planetary Science Letters, 171(3): 411-424.
801 Farley, K., Natland, J., CRAIG, H., 1992. Binary Mixing of Enriched and Undegassed
802 (Primitive-Questionable) Mantle Components (He, Sr, Nd, Pb) in Samoan Lavas. Earth
803 and Planetary Science Letters, 111: 183–199.
804 Faure, G., 1977. Principles of isotope geology. Wiley, New York: pp. 464.
805 Fontignie, D. and Schilling, J.G., 1996. Mantle heterogeneities beneath the South Atlantic: A
806 Nd-Sr-Pb isotope study along the Mid-Atlantic Ridge (3°S-46°S). Earth and Planetary
807 Science Letters, 142(1-2): 209-221.
808 Garcia, M.O., Jorgenson, B., Mahoney, J.J., Ito, E., Irving, A., 1993. An evaluation of
809 temporal geochemical evolution of Loihi seamount lavas: results of Alvin submersible
810 dives. Journal of the Geophysical Research, 98: 357–380.
811 Graham, D.W., Zindler, A., Kurz, M.D., Jenkins, W.J., Batiza, R., Staudigel, H., 1988. He, Pb,
812 Sr and Nd isotope constraints on magma genesis and mantle heterogeneity beneath
813 young Pacific seamounts. Contributions to Mineralogy and Petrology, 99: 446–463.
814 Hall, L.S., Mahoney, J.J., Sinton, J.M., Duncan, R.A., 2006. Spatial and temporal distribution
815 of a C-like asthenospheric component in the Rano Rahi Seamount Field, East Pacific

816 Rise, 15°–19°S. Geochemistry Geophysics Geosystems, 7: doi:10.1029/2005GC000994.
817 Halliday, A., Dickin, A., Fallick, A., Fitton, J., 1988. Mantle Dynamics - a Nd, Sr, Pb and Os
818 Isotopic Study of the Cameroon Line Volcanic Chain. Journal of Petrology, 29: 181–
819 211.
820 Hanan, B.B., Graham, D.W., 1996. Lead and helium isotope evidence from oceanic basalts
821 for a common deep source of mantle plumes. Science, 272: 991–995.
822 Hart, S., 1984. A large-scale isotope anomaly in the Southern Hemisphere mantle. Nature,
823 309: 753–757.
824 Hart, S., 1988. Heterogeneous Mantle Domains: Signatures, Genesis and Mixing
825 Chronologies. Earth and Planetary Science Letters, 90: 273–296.
826 Hart, S., Hauri, E., Oschman, L., Whitehead, J., 1992. Mantle Plumes and Entrainment -
827 Isotopic Evidence. Science, 256: 517–520.
828 Hattori, K., Guillot, S., 2003. Volcanic fronts form as a consequence of serpentinite
829 dehydration in the forearc mantle wedge. Geology, 31: 525–528.
830 Hauff, F., Hoernle, K., Tilton, G., Graham, D.W. and Kerr, A.C., 2000. Large volume
831 recycling of oceanic lithosphere over short time scales : geochemical constraints from
832 the Caribbean Large Igneous Province. Earth and Planetary Science Letters, 174: 247-
833 263.
834 Hémond, C., Arndt, N.T., Lichtenstein, U., Hofmann, A.W., Oskarsson, N. and
835 Steinthorsson, S., 1993. The heterogeneous Iceland plume : Nd-Sr-O isotopes and trace
836 element constraints. Journal of Geophysical Research-Solid Earth, 98(B9): 15833-
837 15850.
838 Hémond, C., Hofmann, A.W., Vlastelic, I. and Nauret, F., 2006. Origin of MORB enrichment
839 and relative trace element compatibilities along the Mid-Atlantic Ridge between 10°
840 and 24°N. Geochemistry Geophysics Geosystems, 7: doi:10.1029/2006GC001317.

841 Hillier, J.K., Watts, A.B., 2007. Global distribution of seamounts from ship-track bathymetry
842 data. Geophysical Research Letters, 34: L13304.
843 Hofmann, A.W., 1988. Chemical differentiation of the Earth: the relationship between mantle,
844 continental crust, and oceanic crust. Earth and Planetary Science Letters, 90(3): 297-314.
845 Hofmann, A.W., 1997. Mantle geochemistry: the message from oceanic volcanism. Nature,
846 385(6613): 219-229.
847 Hofmann, A.W., 2003. Sampling Mantle Heterogeneity through Oceanic Basalts: Isotopes
848 and Trace Elements, Treatise on Geochemistry. Pergamon, Oxford: 61-97.
849 Iwamori, H., 1998. Transportation of H2O and melting in subduction zones. Earth and
850 Planetary Science Letters, 160: 65–80.
851 Jackson, M.G. and Dasgupta, R., 2008. Compositions of HIMU, EM1, and EM2 from global
852 trends between radiogenic isotopes and major elements in ocean island basalts. Earth
853 and Planetary Sciences Letters, 276(1-2): 175-186.
854 Jochum, K.P., Stoll, B., Herwig, K. and Willbold, M., 2007. Validation of LA-ICP-MS trace
855 element analysis of geological glasses using a new solid-state 193 nm Nd: YAG laser
856 and matrix-matched calibration. Journal of Analytical Atomic Spectrometry, 22: 112-
857 121.
858 Koppers, A.A.P., Staudigel, H., Pringle, M.S., Wijbrans, J.R., 2003. Short-lived and
859 discontinuous intraplate volcanism in the South Pacific: hotspots or extensional
860 volcanism? Geochemistry Geophysics Geosystems 4. doi:10.1029/2003GC000533.
861 Koppers, A.A.P., Watts, A.B., 2010. Intraplate Seamounts as a Window into Deep Earth
862 Processes. Oceanography, 23: 42–57.
863 Klein, E.M. and Langmuir, C.H., 1987. Global correlations of ocean ridge basalt chemistry
864 with axial depth and crustal thickness. Journal of Geophysical Research-Solid Earth and
865 Planets, 92(B8): 8089-8115.

Langmuir, C.H., Vocke, R., Hanson, G., Hart, S., 1978. A General Mixing Equation with Applications to Icelandic Basalts. Earth and Planetary Science Letters, 37: 380–392.

Lee, D., Halliday, A., Fitton, J., Giampero, P., 1994. Isotopic variations with distance and time in the volcanic islands of the Cameroon line: evidence for a mantle plume origin. Earth and Planetary Science Letters 123: 119–138.

Leroex, A.P., Dick, H.J.B. and Watkins, R.T., 1992. Petrogenesis of anomalous K-enriched MORB from the Southwest Indian Ridge 11°53'E to 14°38'E. Contributions to Mineralogy and Petrology, 110(2-3): 253-268.

Macdougall, J.D. and Lugmair, G.W., 1986. Sr and Nd isotopes in basalts from the East Pacific Rise - Significance for mantle heterogeneity. Earth and Planetary Science Letters, 77(3-4): 273-284.

Manhès, G., Minster, J.F., and Allègre, C.J., 1978 Comparative uranium-thorium-lead and rubidium-strontium study of the Saint Severin amphoterite: consequences for early solar system chronology. Earth and Planetary Sciences Letters, 39(1): 14-24.

Marske, J.P., Garcia, M.O., Pietruszka, A.J., Rhodes, J.M. and Norman, M.D., 2008. Geochemical variations during Kilauea's Pu'u 'O'o eruption reveal a fine-scale mixture of mantle heterogeneities within the Hawaiian plume. Journal of Petrology, 49(7): 1297-1318.

Marske, J.P., Pietruszka, A.J., Weis, D., Garcia, M.O. and Rhodes, J.M., 2007. Rapid passage of a small-scale mantle heterogeneity through the melting regions of Kilauea and Mauna Loa Volcanoes. Earth and Planetary Science Letters, 259(1-2): 34-50.

McDonough, W.F. and Sun, S.S., 1995. The composition of the Earth. Chemical Geology, 120(3-4): 223-253.

McKenzie, D., Stracke, A., Blichert-Toft, J., Albarède, F., Grönvold, K., and O'Nions, R.K., 2004. Source enrichment processes responsible for isotopic anomalies in oceanic island

basalts. Geochimica et Cosmochimica Acta, 68(12): 2699-2724.

Melson, W., O'Hearn, T. and Jarosewich, E., 2002. A data brief on the Smithsonian Abyssal Volcanic Glass Data file. Geochemistry Geophysics Geosystems, 3(4).

Michael, P.J., Forsyth, D.W., Blackman, D.K., Fox, P.J., Hanan, B.B., Harding, A.J., Macdonald, K.C., Neumann, G.A., Orcutt, J.A., Tolstoy, M.,and Weiland, C.M., 1994. Mantle control of a dynamically evolving spreading center: Mid-Atlantic Ridge 31-34°S. Earth and Planetary Sciences Letters, 121(3-4): 451-468.

Morgan, W.J., 1971. Convection Plumes in the Lower Mantle. Nature, 230: 42–43.

Nauret, F., Abouchami, W., Galer, S.J.G., Hofmann, A.W., Hémond, C., Chauvel, C., Dyment, J., 2006. Correlated trace element-Pb isotope enrichments in Indian MORB along 18-20°S, Central Indian Ridge. Earth and Planetary Science Letters, 245(1-2): 137-152.

Niu, Y.L. and Batiza, R., 1997. Trace element evidence from seamounts for recycled oceanic crust in the eastern Pacific mantle. Earth and Planetary Science Letters, 148(3-4): 471-483.

Niu, Y.L., Collerson, K.D., Batiza, R., Wendt, J.I. and Regelous, M., 1999. Origin of enriched-type mid-ocean ridge basalt at ridges far from mantle plumes: The East Pacific Rise at 11°20'N. Journal of Geophysical Research-Solid Earth, 104(B4): 7067-7087.

Niu, Y.L., Regelous, M., Wendt, I.J., Batiza, R. and O'Hara, M.J., 2002. Geochemistry of near-EPR seamounts: importance of source vs. process and the origin of enriched mantle component. Earth and Planetary Science Letters, 199(3-4): 327-345.

O'Nions, R.K., Hamilton, P.J. and Evensen, N.M., 1977. Variations in $^{143}Nd/^{144}Nd$ and $^{87}Sr/^{86}Sr$ ratios in oceanic basalts. Earth and Planetary Science Letters, 34(1): 13-22.

Plank, T., Langmuir, C.H., 1998. The chemical composition of subducting sediment and its consequences for the crust and mantle. Chemical Geology, 145: 325–394.

916 Richard, P., Shimizu, N. and Allègre, C. J., 1976. $^{143}Nd/^{146}Nd$, a natural tracer: an application to
917 oceanic basalts. Earth and Planetary Science Letters, 31(2): 269-278.
918 Regelous, M., Niu, Y., Wendt, J.I., Batiza, R., Greig, A., and Collerson, K.D., 1999.
919 Variations in the geochemistry of magmatism on the East Pacific Rise at 10°30'N since
920 800 ka. Earth and Planetary Science Letters, 168(1-2): 45-63.
921 Rüpke, L., Morgan, J., Hort, M., Connolly, J., 2004. Serpentine and the subduction zone
922 water cycle. Earth and Planetary Science Letters, 223: 17–34.
923 Schiano, P., Birck, J.L. and Allègre, C.J., 1997. Osmium-strontium-neodymium-lead isotopic
924 covariations in mid-ocean ridge basalt glasses and the heterogeneity of the upper mantle.
925 Earth and Planetary Science Letters, 150(3-4): 363-379.
926 Schilling, J.G., 1973. Iceland mantle plume: Geochemical study of Reykjanes ridge. Nature,
927 242(5400): 565-571.
928 Schilling, J.G., Thompson, G., Kingsley, R. and Humphris, S., 1985. Hotspot-migrating ridge
929 interaction in the South Atlantic. 313(5999): 191.
930 Schilling, J.G., Hanan B.B., McCully B., Kingsley R.H., Fontignie D., 1994. Influence of the
931 Sierra Leone mantle plume on the equatorial Mid-Atlantic Ridge : a Nd-Sr-Pb isotopic
932 study. Journal of Geophysical Research-Solid Earth, 99(B6): 12005-12028.
933 Sims, K.W.W., Blichert-Toft, J., Fornari, D.J., Perfit, M.R., Goldstein, S.J., Johnson, P.,
934 DePaolo, D.J., Hart, S.R., Murrell, M.T., Michael, P.J., Layne, G.D., and Ball, L.A.,
935 2003. Aberrant youth: Chemical and isotopic constraints on the origin of off-axis lavas
936 from the East Pacific Rise, 9°-10°N. Geochemistry Geophysics Geosystems, 4:
937 doi:10.1029/2002GC000443.
938 Stracke, A., Hofmann, A., Hart, S., 2005. FOZO, HIMU, and the rest of the mantle zoo.
939 Geochemistry Geophysics Geosystems 6: doi: 10.1029/2004GC000824.
940 Staudacher, T, Sarda, P., Richardson, S.H., Allègre, C.J., Sagna, I., and Dmitriev, L.V., 1989.

941 Noble gases in basalt glasses from a Mid-Atlantic Ridge topographic high at 14°N:
942 geodynamic consequences. Earth and Planetary Science Letters, 96(1-2): 119-133.
943 Staudigel, H., Park, K., Pringle, M., Rubenstone, J., Smith, W., Zindler, A., 1991. The
944 Longevity of the South-Pacific Isotopic and Thermal Anomaly. Earth and Planetary
945 Science Letters 102, 24–44.
946 Sun, S.S., Nesbitt, R.W. and Sharaskin, A.Y., 1979. Geochemical characteristics of mid-
947 ocean ridge basalts. Earth and Planetary Science Letters, 44(1): 119-138.
948 Tanaka, R. and Nakamura, E., 2005. Boron isotopic constraints on the source of Hawaiian
949 shield lavas. Geochimica et Cosmochimica Acta, 69(13): 3385-3399.
950 Turner, S., Hawkesworth, C., Rogers, N. and King, P., 1997. U-Th isotope disequilibria and
951 ocean island basalt generation in the Azores. Chemical Geology, 139(1-4): 145-164.
952 Vidal P., and Clauer, N., 1981. Pb and Sr isotopic systematics of some basalts and sulfides
953 from the East Pacific Rise at 21 N (project RITA). Earth and Planetary Science Letters,
954 55(2): 237-246.
955 Vlastélic, I., Dosso, L., Bougault, H., Aslanian, D., Geli, L., Etoubleau, J., Bohn, M., Joron,
956 J.L., and Bollinger, C., 2000. Chemical systematics of an intermediate spreading ridge:
957 The Pacific-Antarctic Ridge between 56°S and 66°S. Journal of Geophysical Research-
958 Solid Earth, 105(B2): 2915-2936.
959 von Blanckenburg F., O'Nions, R.K., and Heinz, J.R., 1996. Distribution and sources of pre-
960 anthropogenic lead isotopes in deep ocean water from Fe-Mn crusts. Geochimica et
961 Cosmochimica Acta, 60(24): 4957-4963.
962 Wanless, D.V., Garcia, M.O., Michael Rhodes, J., Weis, D. and Norman, M.D., 2006. Shield-
963 stage alkalic volcanism on Mauna Loa Volcano, Hawaii. Journal of Volcanology and
964 Geothermal Research, 151(1-3): 141-155.
965 Watts, A.B., Sandwell, D.T., Smith, W.H.F., Wessel, P., 2006. Global gravity, bathymetry,

966 and the distribution of submarine volcanism through space and time. Journal of the
967 Geophysical Research, 111: B08408.
968 Wessel, P., 2001. Global distribution of seamounts inferred from gridded Geosat/ERS-1
969 altimetry. Journal of Geophysical Research, 106: 19,431-19,441.
970 White, W.M. and Schilling, J.G., 1978. Nature and origin of geochemical variation in mid-
971 Atlantic ridge basalts from central North-Atlantic. Geochimica et Cosmochimica Acta,
972 42(10): 1501-1516.
973 White, W.M. and Hofmann, A.W., 1982. Sr and Nd isotope geochemistry of oceanic basalts
974 and mantle evolution. Nature, 296(5860): 821-825.
975 White, W.M. and Patchett, J., 1984. Hf-Nd-Sr isotopes and incompatible element abundances
976 in island arcs: implications for magma origins and crust-mantle evolution. Earth and
977 Planetary Science Letters, 67(2): 167-185.
978 White, W., 1985. Sources of Oceanic Basalts - Radiogenic Isotopic Evidence. Geology, 13:
979 115–118.
980 White, W.M., McBirney, A.R. and Duncan, R.A., 1993. Petrology and Geochemistry of the
981 Galapagos Islands: Portrait of a pathological mantle plume. Journal of Geophysical
982 Research-Solid Earth, 98(B11): 19533-19563.
983 Willbold and Stracke, 2006. Trace element composition of mantle end-members: Implications
984 for recycling of oceanic and upper and lower continental crust. Geochemistry
985 Geophysics Geosystems, 7: doi:10.1029/2005GC001005.
986 Zindler, A., Staudigel, H., Batiza, R., 1984. Isotope and trace element geochemistry of young
987 Pacific seamounts: implications for the scale of upper mantle heterogeneity. Earth and
988 Planetary Science Letters, 70: 175–195.
989 Zindler, A. and Hart, S., 1986. Chemical Geodynamics. Annual Review of Earth and
990 Planetary Sciences, 14: 493-571.
991

992

993 **Figure Captions**

994

995 **Figure 1.** Bathymetry of the study area around the Fifteen–Twenty Fracture Zone, from
996 Smith and Sandwell (1997). Red circles localize the US-Japan MODE 98 dive cruise on board
997 R.V. Yokosuka (dives # 4XX) and complementary samples analyzed during this study (see
998 Table 1). White circles localize additional samples from the 15°20'N FZ area published by
999 Hémond et al. [2006) and used in the next figures.

1000

1001 **Figure 2.** Primitive mantle normalized trace element abundances [McDonough and Sun,
1002 1995) and Sr, Nd and Pb isotopes of samples from the 15°20'N FZ area. Atlantic MORB data
1003 are from Agranier et al. [2005). NHRL: Northern Hemisphere Reference Line [Hart, 1984).

1004

1005 **Figure 3.** (La/Sm)C1 normalized ratios, Nd isotope ratios, Pb isotope ratios and along-axis
1006 cross-section versus latitude. Green and yellow squares are data from this study (respectively
1007 from the northern and the southern segments), blue squares represent data from Hémond et al.
1008 [2006), and green dots correspond to additional isotopic data from Agranier et al. [2005). The
1009 along-axis cross-section highlighting the important topographic high (~1 km max) centered at
1010 14°N and extending to the overall southern segment [data from Smith and Sandwell, 1997).
1011 T: Marathon fracture zone; U: Mercurius fracture zone.

1012

1013 **Figure 4.** Sr, Nd and Pb isotopic compositions of seamounts presumed unrelated to hotspot
1014 [so-called "on-ridge" seamounts, Watts et al., 2006; Koppers and Watts, 2010): Line Islands
1015 [Hart, 1988; Garcia et al., 1993), Marshall Islands [Staudigel et al., 1991; Koppers et al.,
1016 2003), Cameroon line [Halliday et al., 1988; Lee et al., 1994), Rano Rahi seamount field [Hall
1017 et al., 2002), EPR seamounts [Graham et al., 1988; Niu et al., 2002). DMM and FOZO field

1018 are respectively from Workman and Hart [2005) and Stracke et al. [2005).

1019

1020 **Figure 5.** Primitive Mantle [PM; McDonough and Sun, 1995) normalized trace element
1021 compositions of two modeled recycled OIB/seamount ("0.05:1" and "0.15:1" red lines),
1022 calculated using the non-modal batch melting equation from Shaw [1970) and the solid binary
1023 mixing model developed by Faure [1977). Assuming that the E-MORB genesis results from
1024 the mixing between the DMM and an enriched component (i.e. the recycled OIB/seamount),
1025 the trace element composition of the E-MORB source is first calculated by "inverting" the E-
1026 MORB composition (the green line). The DMM composition is modeled from the local N-
1027 MORB composition (the blue line) applying 10% of batch melting. Then, two recycled
1028 OIB/seamount compositions are deduced from the calculated E-MORB source and the DMM
1029 compositions using mixing ratios of 0.05:1 and 0.15:1 (the two red lines). These mixing ratios
1030 were chosen so that at least 90% of the PM-normalized trace element contents of the modeled
1031 recycled OIB/seamount plot within OIB field. Our accurate inspection of available OIB data
1032 allowed us to estimate that OIB fields presented in this study represent an almost complete set
1033 of OIB compositions [data from Willbold and Stracke, 2006). Results are given in Table 3,
1034 see the text for more details.

1035

1036 **Figure 6.** Isotope composition of the enriched component calculated using the binary mixing
1037 equation developed by Faure [1977). Isotope ratios of the mixture are those of the most
1038 enriched E-MORB (sample 428R5). Isotopes ratios of the DMM correspond to the regional
1039 average of N-MORB isotope ratios. Two enriched components (large green circles) are
1040 calculated and plotted in each isotope space, depending on the mixing proportions which were
1041 constrained by results of the trace element modeling (i.e. 5% and 15%). Other parameters are
1042 summarized in Table 2 and Table 3. OIB fields are from Willbold and Stracke [2010): HIMU

(in red), EM 1 (in blue), EM 2 (in orange) and FOZO (in green). Colored stars correspond to the average isotopic compositions [Jackson and Dasgupsta, 2008) for each type of OIB, and colored lines are the mixing trends calculated between the DMM and average OIB isotopic compositions, using the same color codes as for the OIB fields. Sr, Nd and Pb elemental compositions of OIB used to calculate the mixing trends are from Willbold and Stracke [2006).

Figure 7. Binary mixing modeling between a recycled OIB/seamount and the N-MORB source applied on the samples from the 18°S region of the CIR [Nauret et al., 2006). Parameters, given in Table 2 and 3, were determined by the same way as for the MAR modeling. See the text and the Figure 6 caption for more details about the modeling.

Figure 8. Histograms showing variations and frequencies of Sr/Nd, Sr/Pb and Nd/Pb elemental ratios of MORB and EM-1, EM-2, HIMU and FOZO OIB (the group OIB in yellow corresponds to the addition of the four OIB subgroups). MORB are compiled from the LDEO petrological database at http://petdb.ldeo.columbia.edu/petdb (see Tables S4 and S5 for data, selecting criteria and references). OIB data are from Willbold and Stracke [2006). The formula for the K parameter is given in the section 5.4 of the discussion.

Figure 9. Evolution of $^{206}Pb/^{204}Pb$ and $^{208}Pb/^{204}Pb$ composition with time of modeled recycled OIB/seamount, the DMM and the "D-DMM", using the isotopic decay equations $(^{206}Pb/^{204}Pb)=(^{206}Pb/^{204}Pb)_t + \mu(e^{\lambda 238 t}-1)$ and $(^{208}Pb/^{204}Pb)=(^{208}Pb/^{204}Pb)_t + \kappa(e^{\lambda 232 t}-1)$, where t is the time, μ is the $^{238}U/^{204}Pb$ ratio, κ is the $^{232}Th/^{238}U$ ratio, and λ^{238} and λ^{232} are the decay constants respectively for ^{238}U and ^{232}Th. Parameters are given in Table 2 and in Table S3. DMM Pb isotope compositions are from Su and Langmuir [2003) and correspond to a global average of

1068 N-MORB isotopic compositions from the MAR, CIR and EPR. D-DMM is calculated based
1069 on the isotopes that are 2σ depleted from the average, as calculated by Workman and Hart
1070 [2005). Ages given by line intersections are interpreted as the maximum age of the recycled
1071 OIB/seamount, considering that the recycled OIB/seamount cannot be more depleted than the
1072 DMM.
1073
1074 **Figure 10.** Sketch of E-MORB genesis (not at scale). The seamount is subducted and
1075 recycled with some of the oceanic crust into the upper mantle following the mantle
1076 convection to finish below a ridge segment to form E-MORB. As a complete mantle overturn
1077 (transit to core-mantle boundary and back to surface) is expected to be 400-500 Myr [Tackley,
1078 2000], the ~250 Myr age calculated from isotope data suggests that parts of OIB are likely
1079 recycled within the upper mantle.

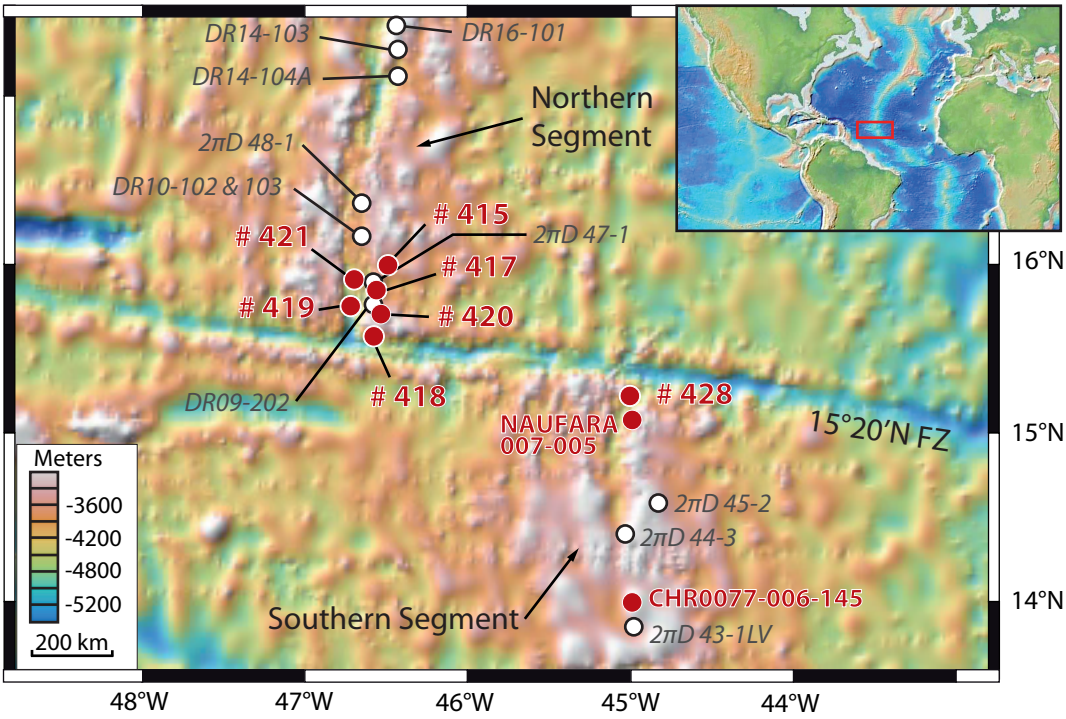
DR14-103
DR16-101
DR14-104A
Northern
Segment
2πD 48-1
DR10-102 & 103
415
421
2πD 47-1
417
419
420
418
DR09-202
428
NAUFARA
007-005
15°20'N FZ
2πD 45-2
2πD 44-3
Southern Segment
CHR0077-006-145
2πD 43-1LV
Meters
-3600
-4200
-4800
-5200
200 km
16°N
15°N
14°N
48°W
47°W
46°W
45°W
44°W

Figure 1

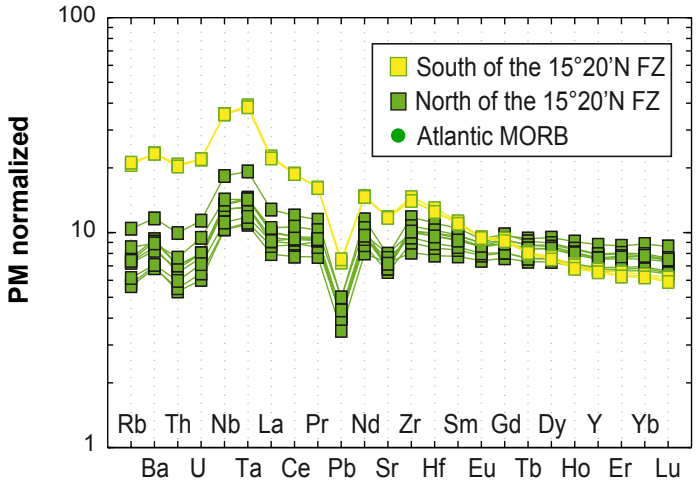
PM normalized
100
10
1
South of the 15°20'N FZ
North of the 15°20'N FZ
Atlantic MORB
Rb Th Nb La Pr Nd Zr Sm Gd Dy Y Yb
Ba U Ta Ce Pb Sr Hf Eu Tb Ho Er Lu

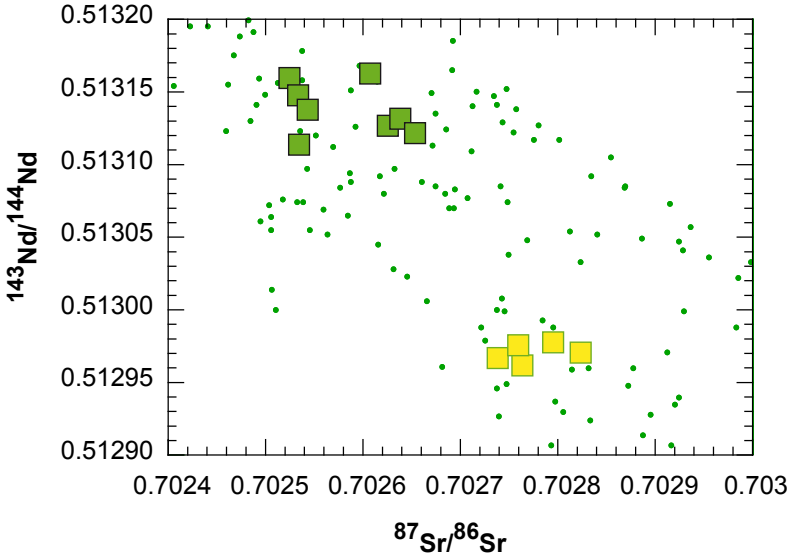
143Nd/144Nd
0.51320
0.51315
0.51310
0.51305
0.51300
0.51295
0.51290
0.7024 0.7025 0.7026 0.7027 0.7028 0.7029 0.703
87Sr/86Sr

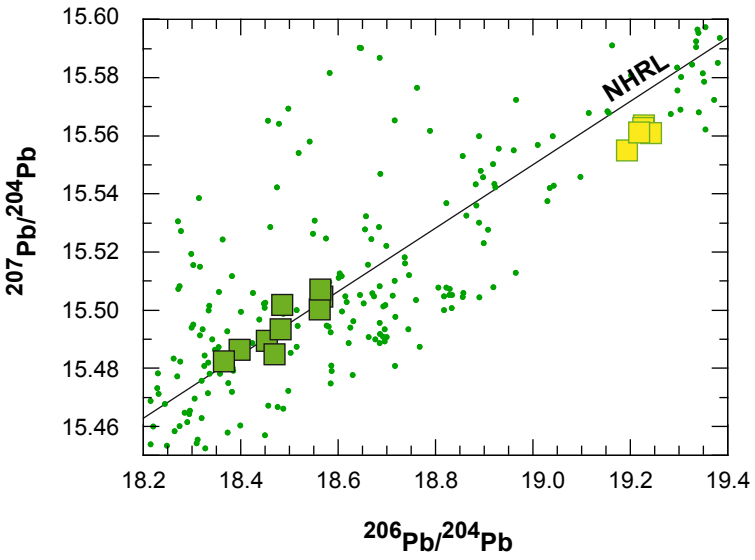
207Pb/204Pb
15.60
15.58
15.56
15.54
15.52
15.50
15.48
15.46
NHRL
18.2 18.4 18.6 18.8 19.0 19.2 19.4
206Pb/204Pb

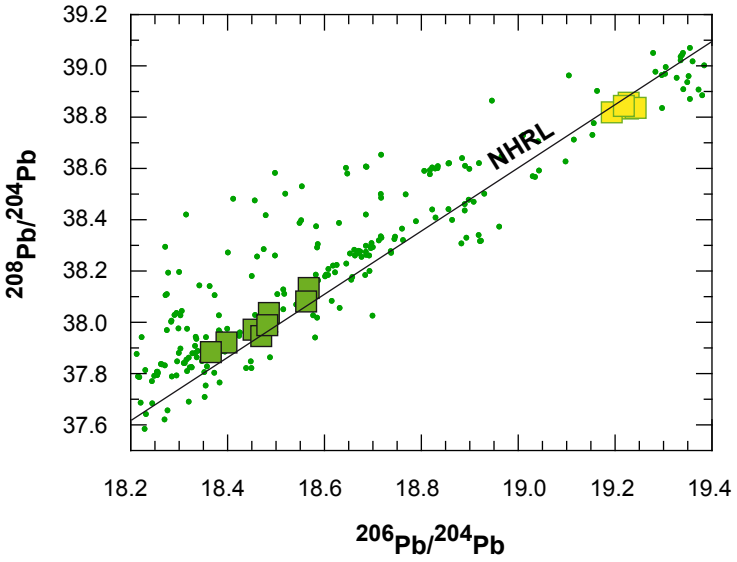
208Pb/204Pb
39.2
39.0
38.8
38.6
38.4
38.2
38.0
37.8
37.6
NHRL
18.2 18.4 18.6 18.8 19.0 19.2 19.4
206Pb/204Pb

Figure 2

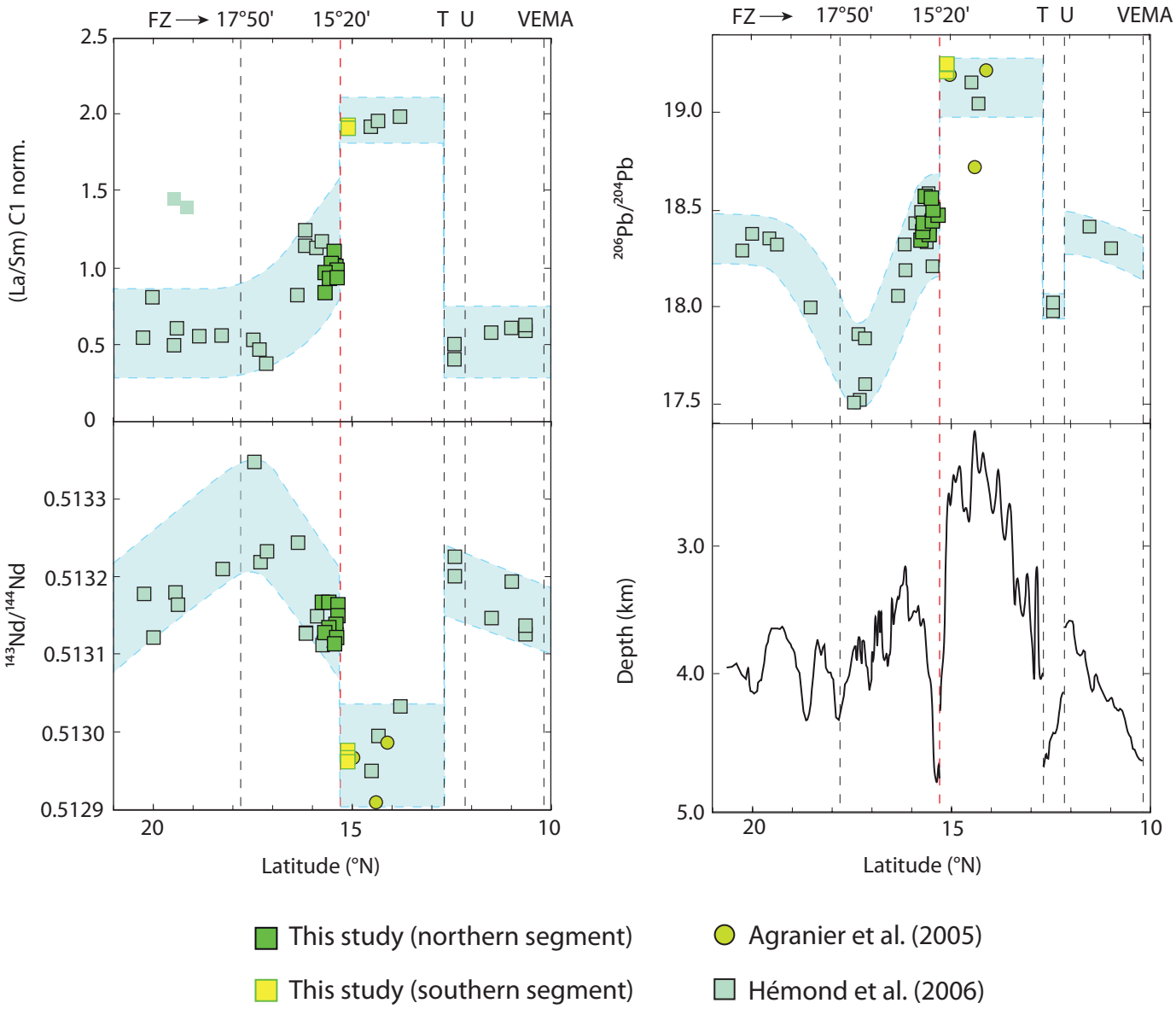
FZ → 17°50'
15°20'
T U
VEMA
(La/Sm) C1 norm.
143Nd/144Nd
206Pb/204Pb
Depth (km)
Latitude (°N)
This study (northern segment)
This study (southern segment)
Agranier et al. (2005)
Hémond et al. (2006)

Figure 3

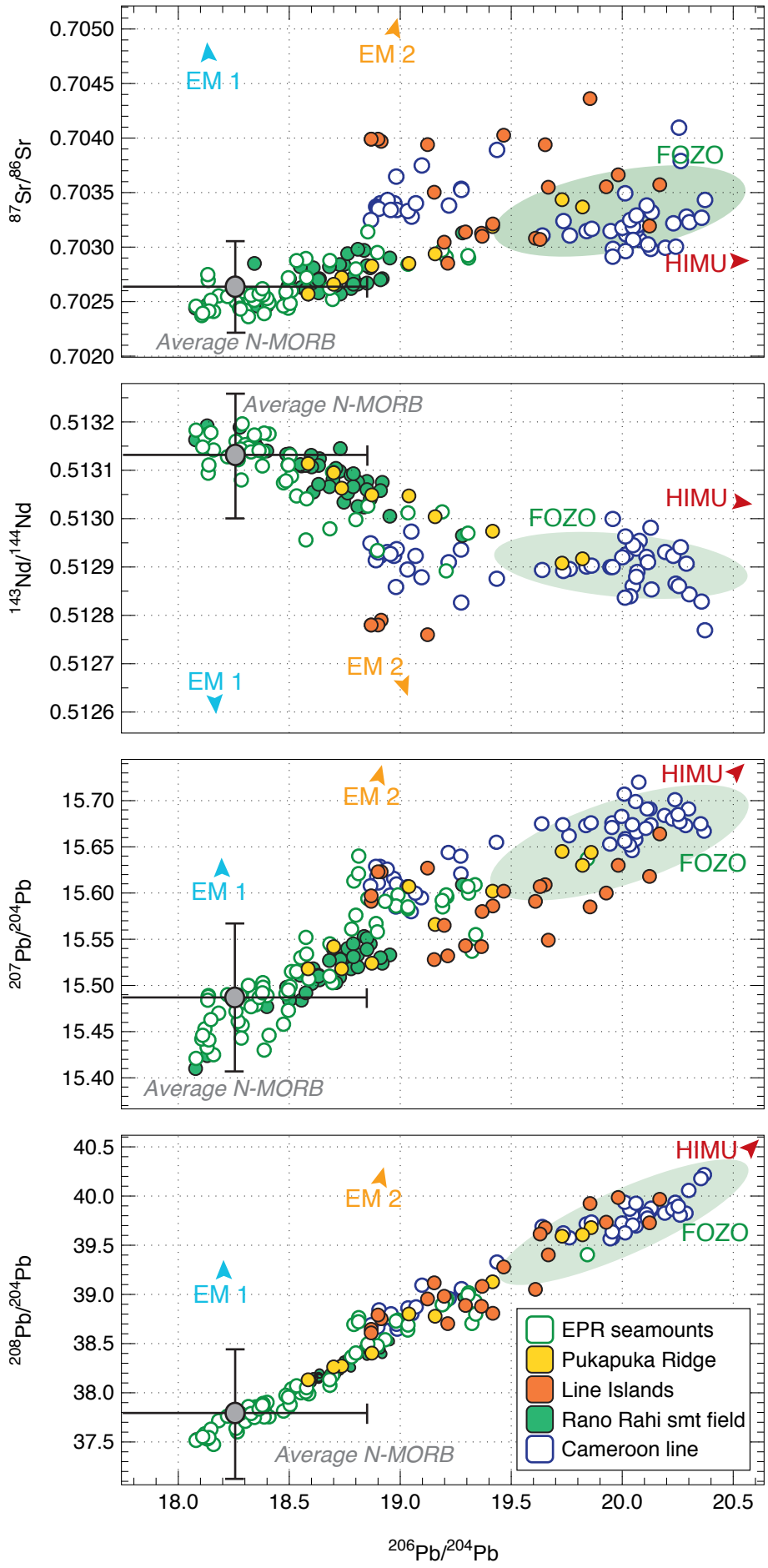
0.7050
0.7045
0.7040
0.7035
0.7030
0.7025
0.7020
87Sr/86Sr
EM 1
EM 2
FOZO
HIMU
Average N-MORB
0.5132
0.5131
0.5130
0.5129
0.5128
0.5127
0.5126
143Nd/144Nd
Average N-MORB
HIMU
FOZO
EM 2
EM 1
15.70
15.65
15.60
15.55
15.50
15.45
15.40
207Pb/204Pb
HIMU
EM 2
FOZO
EM 1
Average N-MORB
40.5
40.0
39.5
39.0
38.5
38.0
37.5
208Pb/204Pb
HIMU
EM 2
FOZO
EM 1
Average N-MORB
EPR seamounts
Pukapuka Ridge
Line Islands
Rano Rahi smt field
Cameroon line
18.0
18.5
19.0
19.5
20.0
20.5
206Pb/204Pb

Figure 4

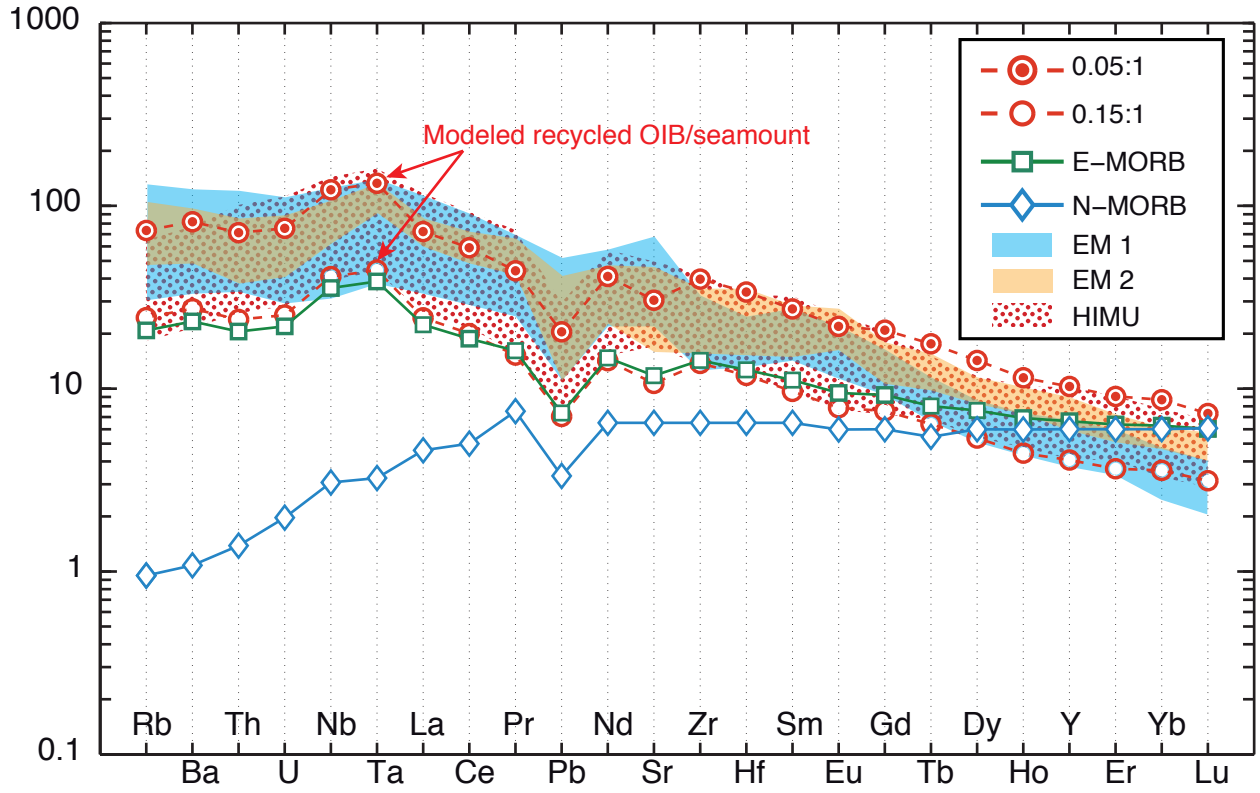
1000
100
10
1
0.1
Modeled recycled OIB/seamount
0.05:1
0.15:1
E–MORB
N–MORB
EM 1
EM 2
HIMU
Rb
Ba
Th
U
Nb
Ta
La
Ce
Pr
Pb
Nd
Sr
Zr
Hf
Sm
Eu
Gd
Tb
Dy
Ho
Y
Er
Yb
Lu

Figure 5

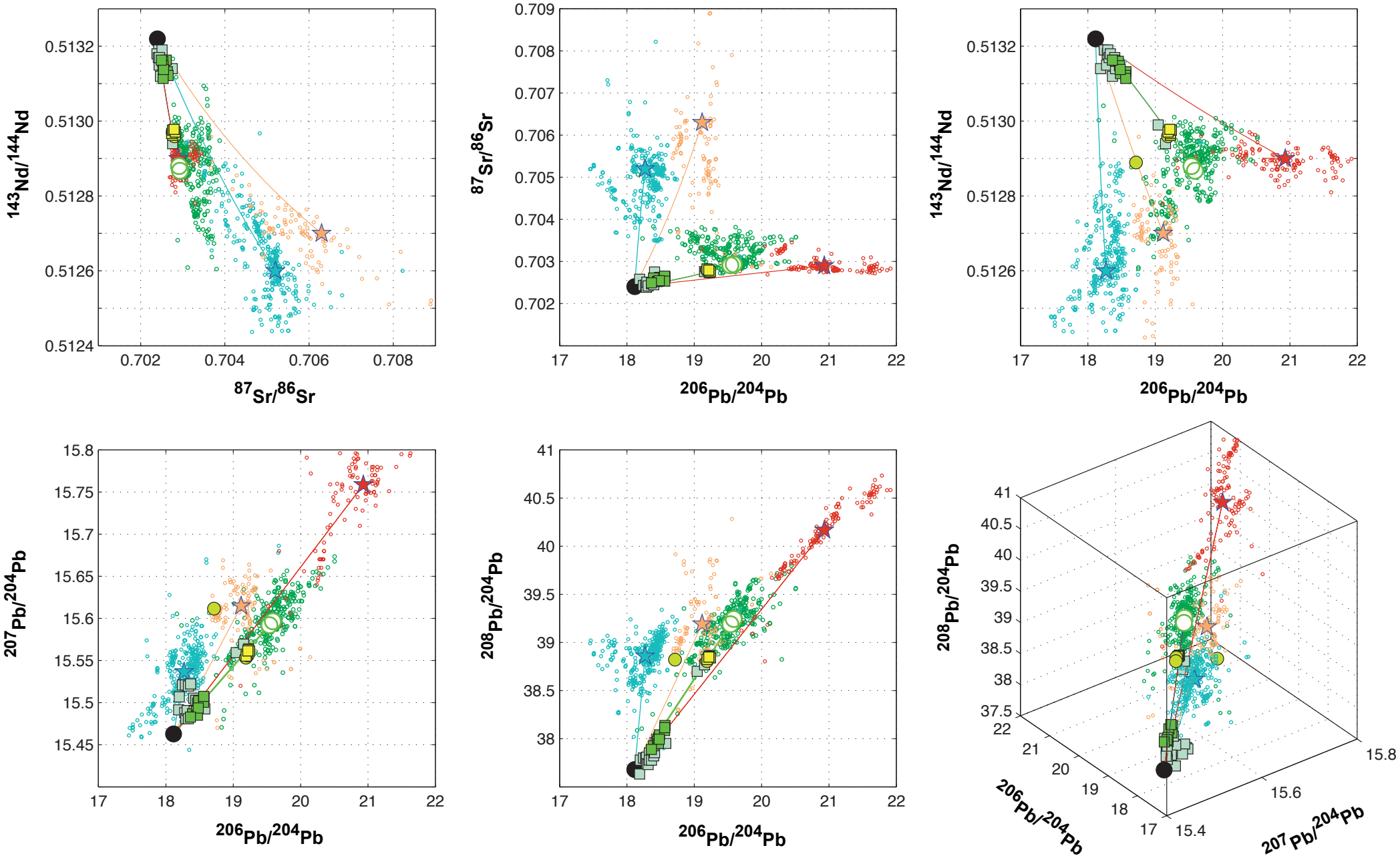
143Nd/144Nd
87Sr/86Sr
87Sr/86Sr
206Pb/204Pb
143Nd/144Nd
206Pb/204Pb
207Pb/204Pb
206Pb/204Pb
208Pb/204Pb
206Pb/204Pb
208Pb/204Pb
206Pb/204Pb
207Pb/204Pb
EM 1
EM 2
HIMU
FOZO
Agranier et al. (2005)
Hémond et al. (2006)
This study (North and South)
DMM
Modeled recycled OIB/seamount

Figure 6

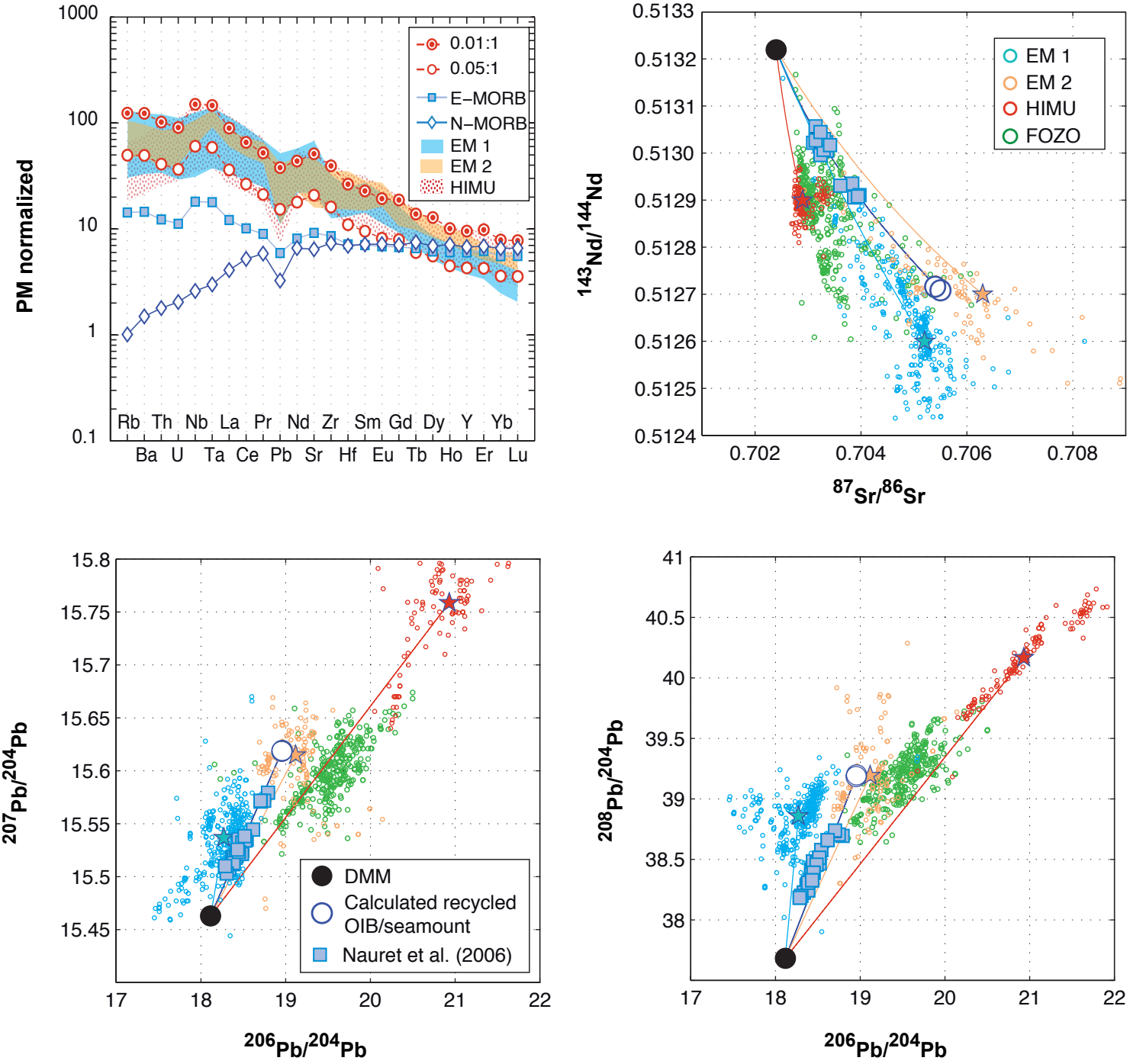
PM normalized
1000
100
10
1
0.1
0.01:1
0.05:1
E–MORB
N–MORB
EM 1
EM 2
HIMU
Rb Th Nb La Pr Nd Zr Sm Gd Dy Y Yb
Ba U Ta Ce Pb Sr Hf Eu Tb Ho Er Lu
143Nd/144Nd
0.5133
0.5132
0.5131
0.5130
0.5129
0.5128
0.5127
0.5126
0.5125
0.5124
EM 1
EM 2
HIMU
FOZO
0.702
0.704
0.706
0.708
87Sr/86Sr
207Pb/204Pb
15.8
15.75
15.7
15.65
15.6
15.55
15.5
15.45
DMM
Calculated recycled OIB/seamount
Nauret et al. (2006)
17
18
19
20
21
22
206Pb/204Pb
208Pb/204Pb
41
40.5
40
39.5
39
38.5
38
17
18
19
20
21
22
206Pb/204Pb

Figure 7

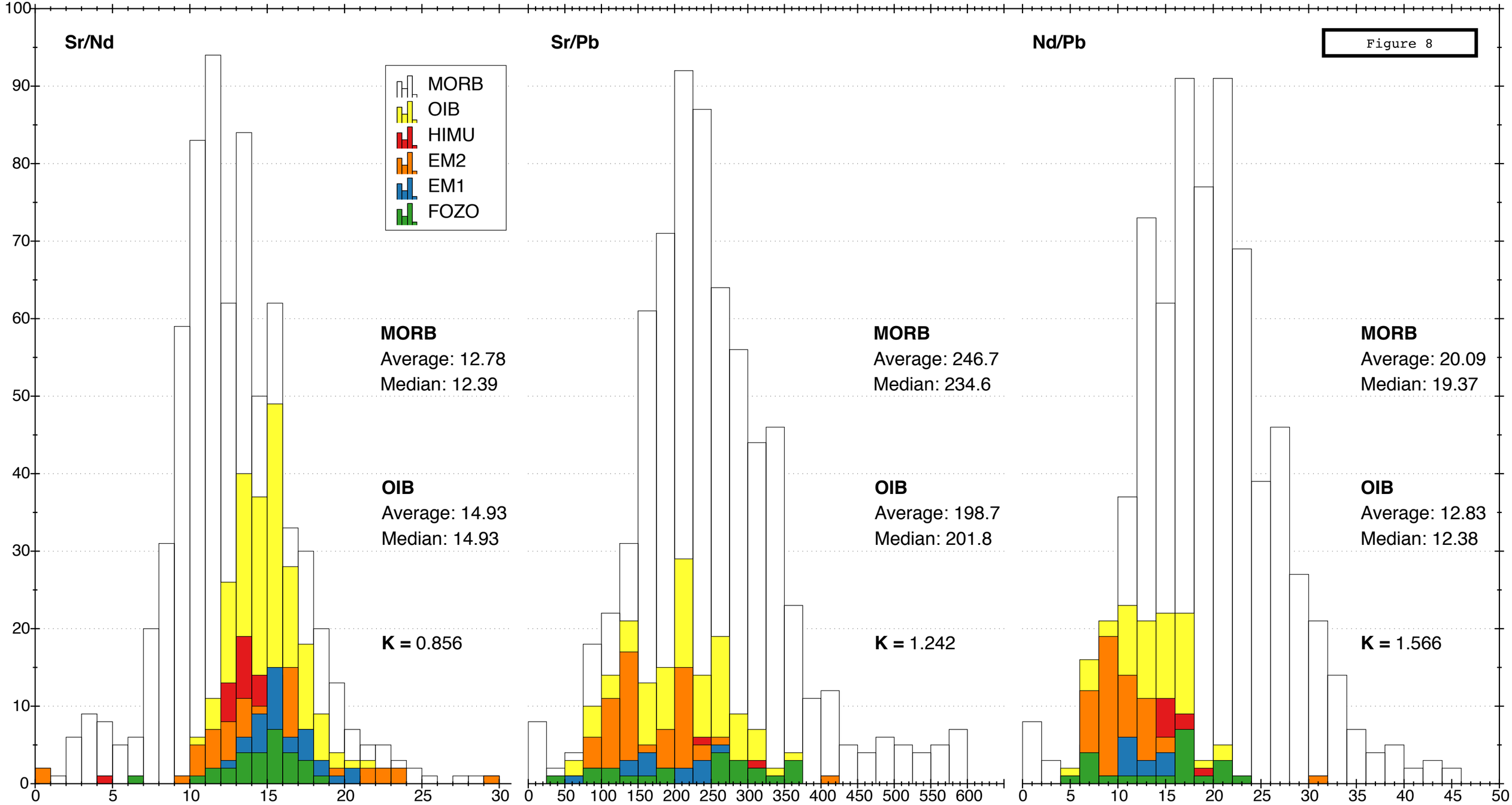
Figure 8
Sr/Nd
Sr/Pb
Nd/Pb
MORB
OIB
HIMU
EM2
EM1
FOZO
MORB
Average: 12.78
Median: 12.39
OIB
Average: 14.93
Median: 14.93
K = 0.856
MORB
Average: 246.7
Median: 234.6
OIB
Average: 198.7
Median: 201.8
K = 1.242
MORB
Average: 20.09
Median: 19.37
OIB
Average: 12.83
Median: 12.38
K = 1.566

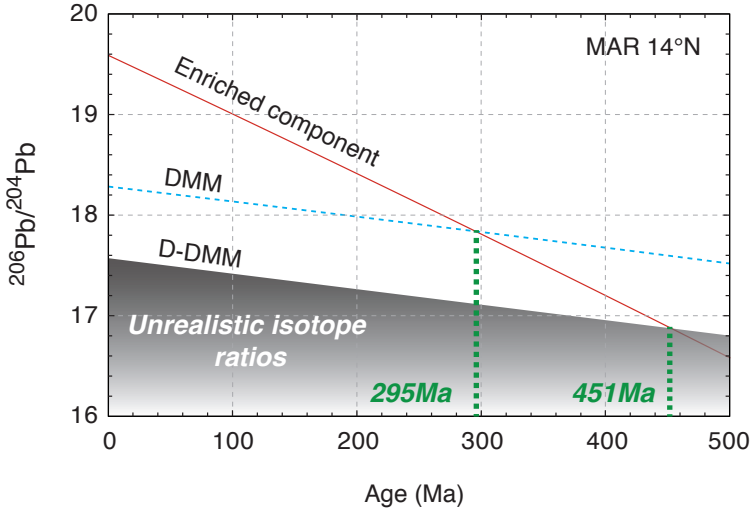
MAR 14°N
Enriched component
DMM
D-DMM
Unrealistic isotope ratios
295Ma
451Ma
$^{206}Pb/^{204}Pb$
Age (Ma)

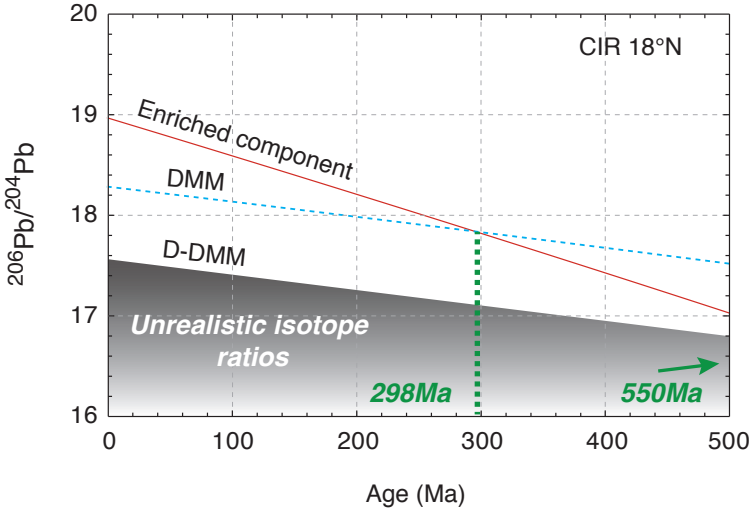
CIR 18°N
Enriched component
DMM
D-DMM
Unrealistic isotope ratios
298Ma
550Ma
$^{206}Pb/^{204}Pb$
Age (Ma)

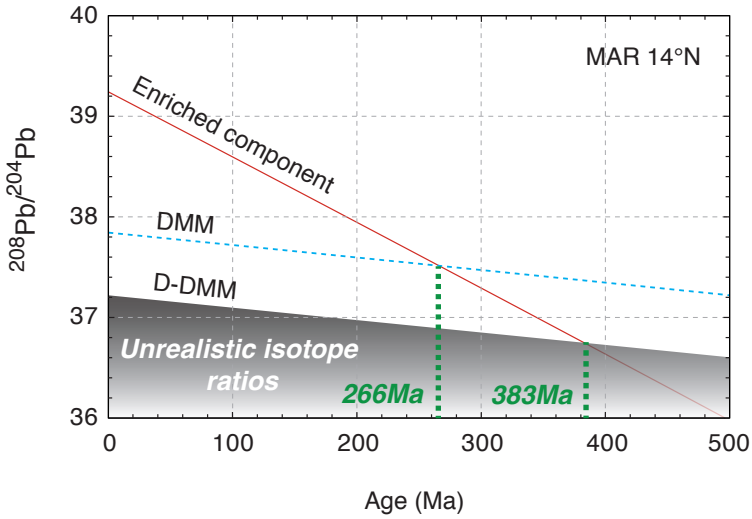
MAR 14°N
Enriched component
DMM
D-DMM
Unrealistic isotope ratios
266Ma
383Ma
$^{208}Pb/^{204}Pb$
Age (Ma)

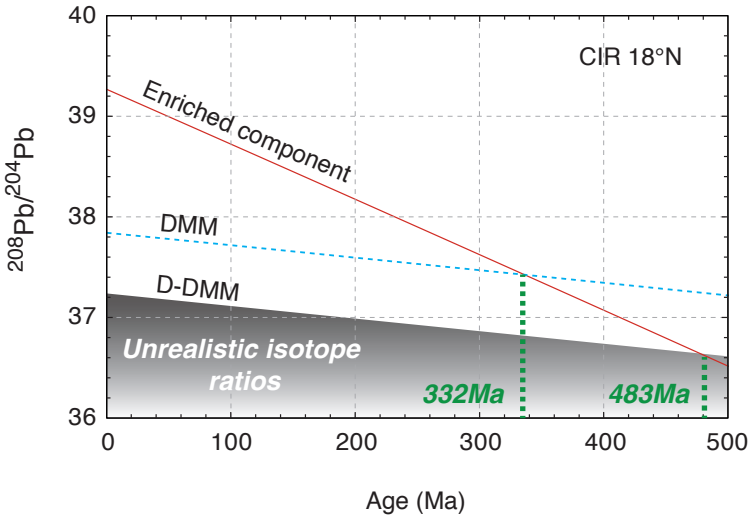
CIR 18°N
Enriched component
DMM
D-DMM
Unrealistic isotope ratios
332Ma
483Ma
$^{208}Pb/^{204}Pb$
Age (Ma)

Figure 9

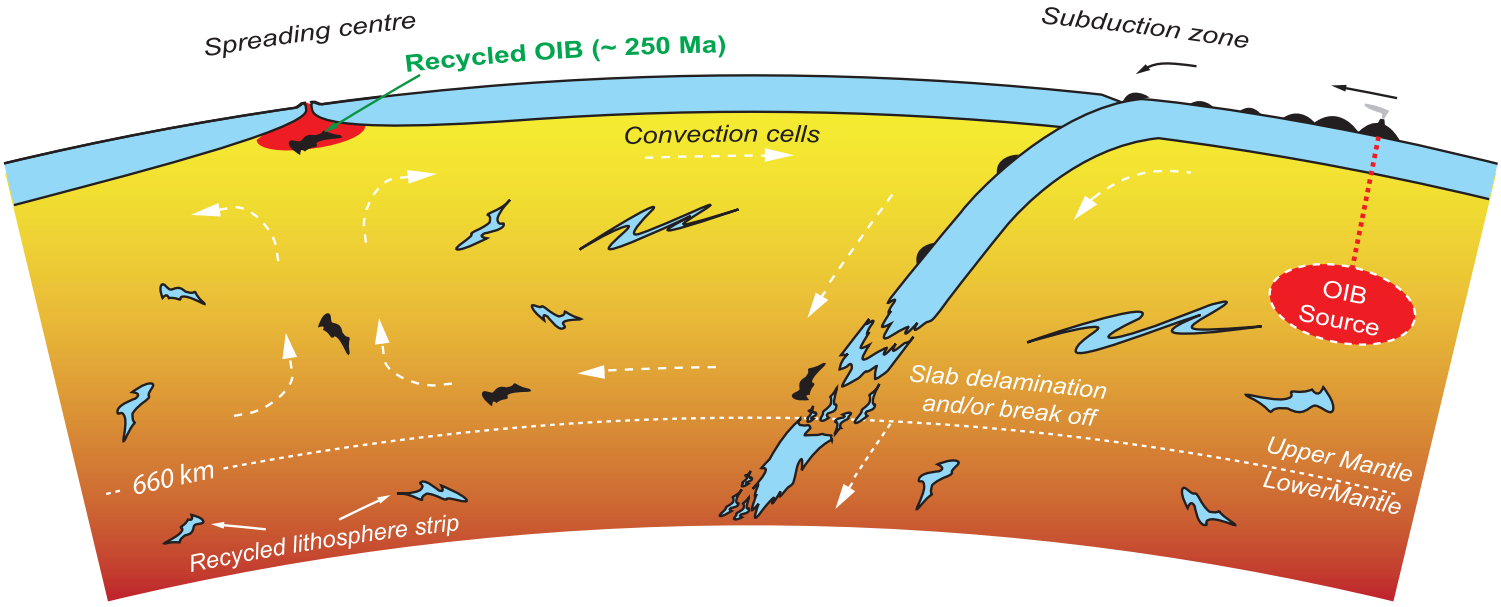
Spreading centre
Recycled OIB (~ 250 Ma)
Subduction zone
Convection cells
OIB
Source
Slab delamination
and/or break off
660 km
Upper Mantle
LowerMantle
Recycled lithosphere strip

Figure 10

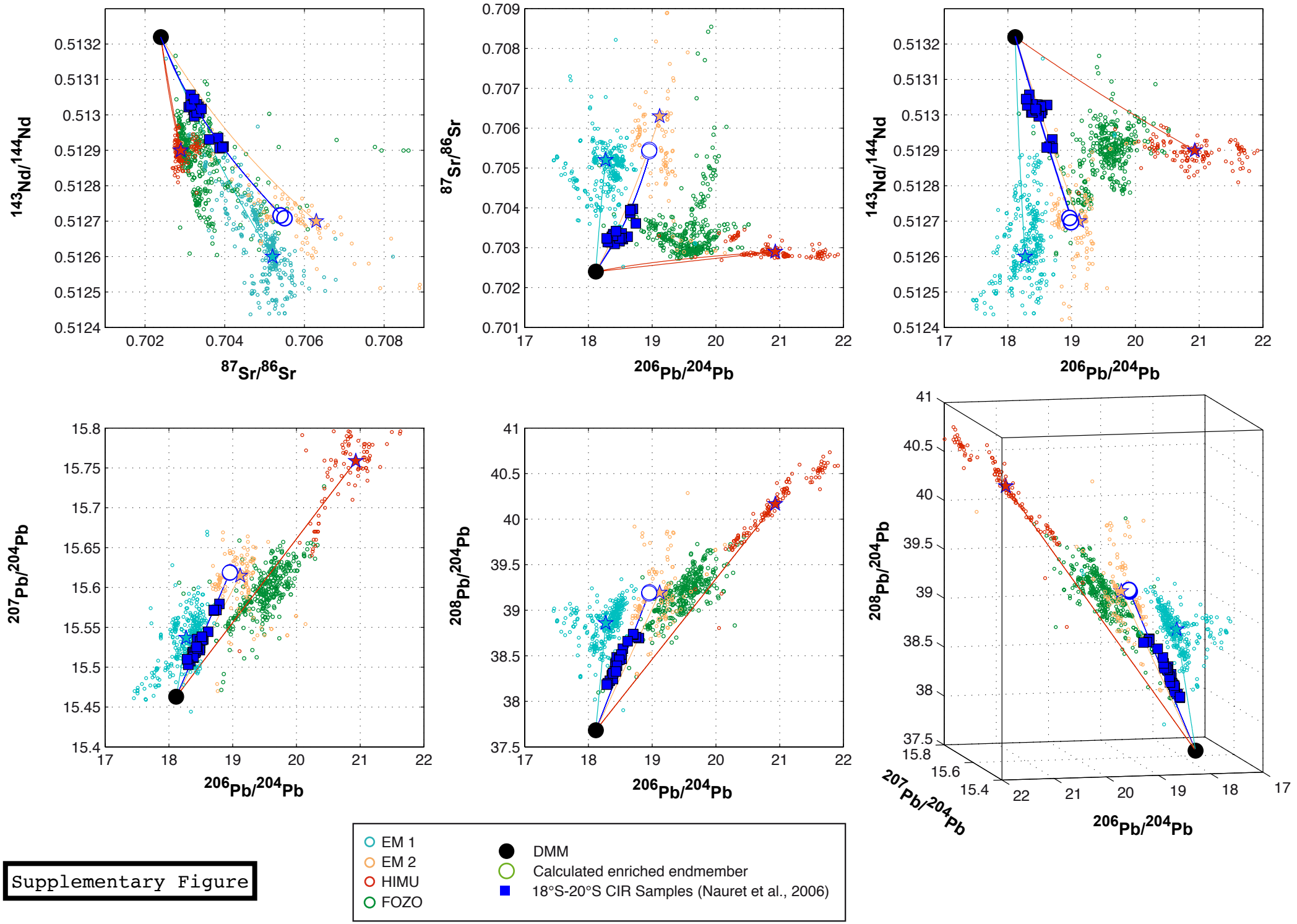

Supplementary Figure

	415R4	415R5	417R1	418R1A	418R3	419R4	419R11	420R7	421R1	428R3	428R4	428R5	NAUFARA-007-005	CHR0077-006-145
Localisation	North of the 15°20'N Fracture Zone									South of the 15°20'N Fracture Zone				
Latitude (°N)	15°39.001	15°39.001	15°39.001	15°20.589	15°20.589	15°25.121	15°25.479	15°22.479	15°31.479	15°07.480	15°07.480	15°07.480	15°01.479	14°07.119
Longitude(°W	46°38,673	46°38,630	46°34,714	46°37,460	46°38,214	46°40,209	46°40,959	46°35,026	46°37,730	44°50,985	44°51,214	44°51,325	44°55.479	45°00.359
SiO_2	50.51	50.82	51.26	50.72	51.08	51.22	50.95	50.74	50.89	51.35	51.33	51.38	*50.30*	
Al_2O_3	15.39	15.85	15.04	14.85	14.56	15.09	15.10	14.79	14.59	14.83	14.55	14.76	*15.34*	
FeO	9.27	9.65	9.59	9.31	9.67	9.25	8.95	9.67	9.77	9.66	9.28	9.51	*9.20*	
MnO	0.17	0.20	0.16	0.18	0.18	0.17	0.21	0.17	0.20	0.15	0.17	0.15	-	
MgO	8.15	6.61	7.85	8.22	7.90	8.08	8.20	7.49	7.62	6.68	6.41	6.53	*8.14*	
CaO	11.14	11.08	10.28	10.67	10.44	10.81	10.73	10.61	10.46	10.35	10.32	10.27	*11.21*	
Na_2O	2.63	3.02	2.85	2.86	2.96	2.94	2.84	2.88	2.91	2.88	2.80	2.81	*2.40*	
K_2O	0.19	0.18	0.23	0.24	0.28	0.26	0.26	0.23	0.21	0.66	0.65	0.66	*0.41*	
TiO_2	1.24	1.46	1.52	1.55	1.69	1.58	1.45	1.63	1.59	1.75	1.71	1.76	*1.36*	
P_2O_5	0.14	0.14	0.20	0.17	0.20	0.16	0.16	0.20	0.19	0.27	0.27	0.24	*0.20*	
Cr_2O_3	0.04	0.06	0.06	0.06	0.04	0.04	0.03	0.05	0.03	0.04	0.04	0.04	-	
Total	98.88	99.11	98.97	98.83	99.01	99.61	98.88	98.47	98.48	98.63	97.55	98.11	*98.56*	
Mg#	0.47	0.41	0.45	0.47	0.45	0.47	0.48	0.44	0.44	0.41	0.41	0.41	0.47	
$Na_{8,0}$	2.69	2.50	2.80	2.94	2.92	2.98	2.92	2.69	2.78	2.39	2.22	2.27	2.45	
Ca	79608	79222	73451	76284	74599	77267	76682	75834	74791	73939	73768	73391		
Co	41.6	43.2	40.0	40.5	38.9	41.1	39.3	40.0	40.4	35.8	34.9	36.6		
Ni	141	106	138	137	119	149	137	108	106	81.5	74.3	85.7		
Cu	87.4	84.3	70.0	65.8	59.9	66.7	65.1	65.6	63.1	58.4	58.6	59.9		
Ga	15.2	16.1	15.3	15.7	15.7	15.0	14.4	15.9	15.4	15.7	15.5	16.0		
Ge	1.24	1.33	1.22	1.27	1.25	1.23	1.22	1.25	1.26	1.25	1.23	1.26		
Rb	3.47	3.38	4.41	4.34	6.26	4.55	4.43	5.13	3.69	12.4	12.4	12.7		
Sr	144	139	130	135	156	159	152	135	143	235	235	233		
Y	27.5	36.0	28.6	32.8	33.4	31.4	28.0	32.2	31.7	27.2	28.1	26.9		
Zr	84.7	106	94.2	107	124	105	99.6	113	106	149	153	147		
Nb	6.81	6.82	8.49	8.41	12.1	8.90	8.83	9.38	7.33	23.3	23.4	23.4		
Mo	0.436	0.447	0.517	0.553	0.715	0.527	0.529	0.567	0.489	1.22	1.22	1.24		
Cd	0.166	0.180	0.175	0.164	0.190	0.187	0.154	0.168	0.196	0.209	0.144	0.156		
In	0.074	0.092	0.082	0.083	0.086	0.079	0.074	0.082	0.086	0.082	0.082	0.084		
Sn	1.30	1.47	1.37	1.48	1.53	1.41	1.35	1.56	1.44	1.72	1.70	1.67		
Sb	0.050	0.051	0.057	0.046	0.090	0.113	0.094	0.062	0.105	0.364	0.193	0.104		
Cs	0.037	0.034	0.040	0.041	0.061	0.038	0.037	0.059	0.033	0.126	0.121	0.123		
Ba	46.0	45.0	56.3	54.3	76.8	61.6	60.0	58.8	46.7	154	154	154		
La	5.14	5.61	5.89	6.13	8.29	6.53	6.48	6.81	5.91	14.5	14.7	14.3		
Ce	13.0	14.7	14.9	15.5	20.1	16.0	16.0	17.9	15.7	31.4	31.5	31.4		
Pr	1.96	2.30	2.18	2.34	2.92	2.41	2.33	2.61	2.37	4.09	4.11	4.09		
Nd	10.0	12.0	10.9	12.0	14.4	12.2	11.7	13.1	12.1	18.4	18.5	18.3		
Sm	3.15	3.91	3.37	3.81	4.25	3.75	3.48	3.97	3.73	4.52	4.58	4.46		
Eu	1.14	1.38	1.20	1.33	1.44	1.32	1.23	1.37	1.34	1.46	1.46	1.45		
Gd	4.13	5.27	4.38	5.02	5.34	4.84	4.39	5.05	4.84	5.01	5.10	4.96		
Tb	0.724	0.929	0.752	0.865	0.902	0.833	0.748	0.865	0.837	0.795	0.802	0.789		
Dy	4.93	6.38	5.11	5.90	6.03	5.65	5.07	5.80	5.68	5.11	5.20	5.06		
Ho	1.03	1.35	1.06	1.24	1.25	1.18	1.06	1.21	1.19	1.03	1.05	1.01		
Er	3.01	3.99	3.12	3.58	3.61	3.41	3.07	3.47	3.45	2.91	2.95	2.86		
Tm	0.432	0.576	0.446	0.512	0.520	0.490	0.440	0.501	0.497	0.407	0.419	0.405		
Yb	2.93	3.90	3.05	3.44	3.50	3.32	3.01	3.40	3.44	2.77	2.81	2.73		
Lu	0.433	0.582	0.446	0.507	0.515	0.494	0.437	0.501	0.506	0.405	0.417	0.397		
Hf	2.21	2.81	2.40	2.81	3.13	2.73	2.52	2.90	2.72	3.55	3.68	3.53		
Ta	0.403	0.411	0.483	0.488	0.712	0.538	0.528	0.528	0.438	1.42	1.45	1.42		
W	0.079	0.077	0.102	0.101	0.136	0.106	0.101	0.114	0.083	0.249	0.251	0.257		
Tl	0.0116	0.018	0.017	0.012	0.019	0.018	0.013	0.024	0.014	0.033	0.023	0.024		
Pb	0.524	0.598	0.613	0.600	0.743	0.645	0.595	0.750	0.652	1.10	1.09	1.13		
Bi	0.011	0.010	0.010	0.009	0.012	0.011	0.008	0.010	0.011	0.015	0.010	0.009		
Th	0.423	0.438	0.518	0.539	0.792	0.561	0.559	0.608	0.474	1.63	1.65	1.61		
U	0.122	0.131	0.155	0.163	0.231	0.161	0.163	0.192	0.145	0.444	0.445	0.446		
$^{87}Sr/^{86}Sr$	0.702625±3	0.702607±8	0.702638±9	0.702524±1	0.702533±2	0.702653±8	0.702534±9	0.702543±9	0.702493±9	0.702763±8	0.702738±5	0.702759±8	0.702823±8	0.702795±4
$^{143}Nd/^{144}Nd$	0.513127±2	0.513163±8	0.513132±7	0.51316±11	0.513148±2	0.513122±9	0.513114±9	0.513138±1	0.513163±9	0.512962±9	0.512967±9	0.512976±7	0.512971±3	0.512978±4
εNd	25.223	25.926	25.321	25.868	25.633	25.125	24.969	25.438	25.926	21.999	22.097	22.273	22.175	22.312
$^{206}Pb/^{204}Pb$	18.4848±21	18.3967±16	18.5668±28	18.4531±19	18.4689±33	18.5614±26	18.5624±28	18.4809±19	18.3647±16	19.2274±19	19.2259±17	19.2413±22	*19.1924*	*19.2172*
$^{207}Pb/^{204}Pb$	15.5021±7	15.4867±5	15.5051±9	15.4898±7	15.4851±10	15.5005±7	15.5075±9	15.4936±7	15.4828±6	15.5638±6	15.5630±5	15.5613±6	*15.5552*	*15.5614*
$^{208}Pb/^{204}Pb$	38.040±0.7	37.927±0.6	38.138±1	37.975±0.7	37.950±1	38.085±0.7	38.115±0.8	37.994±0.8	37.889±0.6	38.860±0.5	38.857±0.4	38.840±0.7	*38.823*	*38.849*

Table 1 : Localisation, major elements, trace elements and isotopic data of samples from the 15°20'N Fz area analysed in this study (see the text for more details on analyses). Additional data in italic are from Melson et al. (2002) for the major elements and from Agranier et al. (2005) for the lead isotopes.

Table 2: References of data used in modelings (#values given in Table 3; *values given in supplementary Table 1)

Trace element modeling	
Partition coefficient	Niu and Hékinian (1997)*
	Donnelly et al. (2004)*
Partial melting degrees (F)	Hémond et al. (2006)*
Mixing proportion	Driven by OIB fields (see text for details)
DMM	Regional N-MORB average (PetDB)#
EM1, EM2 and HIMU fields	Stracke et al. (2003); Willbold and Stracke (2006)
FOZO Austral-Cook	Stracke et al. (2003)
FOZO Azores, Cape Verde, Canary, Cameroon Line, Pukapuka Ridge, Rano-Rahi seamounts	GEOROC database http://georoc.mpch-mainz.gwdg.de/georoc/
Isotope modeling	
Mixing proportion	Driven by OIB fields (see text for details)
Sr, Nd, Pb composition of enriched component	Trace element modeling results #
DMM	North Atlantic N-MORB average (Agranier et al., 2005) #
EM1, EM2 and HIMU fields	Willbold and Stracke (2010)
EM1, EM2 and HIMU averages (Stars in Figures 6 and 7)	Jackson and Dasgupta (2008)*
Elemental Sr, Nd and Pb concentrations in EM1, EM2 and HIMU sources	Willbold and Stracke (2006)*
FOZO Austral-Cook	Stracke et al. (2005)
FOZO Azores, Cape Verde, Canary, Cameroon Line, Pukapuka Ridge, Rano-Rahi seamounts	GEOROC database http://georoc.mpch-mainz.gwdg.de/georoc/
Age	
Enriched endmember	Calculated from isotopic modeling
DMM isotope values	Su and Langmuir (2003)*
Highly DMM	Workman and Hart (2005) after Su and Langmuir (2003)*
µDMM	Elliot et al. (1999)*
κDMM	

Table 3: Resuts of trace element and isotopic modeling

	Mid-Atlantic Ridge (14°N)			Central Indian Ridge (18°-20°S)		
	N-MORB	Modeled OIB		N-MORB	Modeled OIB	
Elements	average	0.05:1	0.15:1	average	0.01:1	0.05:1
Rb	0.571	44.0	14.7	0.613	50.1	30.1
Ba	7.13	541	181	9.99	550	330
Th	0.112	5.67	1.90	0.144	5.48	3.29
U	0.041	1.53	0.512	0.042	1.25	0.749
Nb	2.02	80.4	26.9	1.73	66.7	40.1
Ta	0.123	4.92	1.65	0.112	3.66	2.20
La	2.98	46.8	15.8	2.68	39.2	23.7
Ce	8.38	98.7	33.5	8.84	74.3	45.0
Pr	1.91	11.2	3.87	1.50	8.96	5.44
Pb	0.5	3.07	1.06	0.494	3.84	2.33
Nd	8.13	51.4	17.8	8.35	32.4	19.8
Sr	129	607	212	129	689	419
Zr	68.3	418	145	78.1	280	172
Hf	1.84	9.55	3.34	1.99	5.06	3.14
Sm	2.64	11.1	3.93	2.94	6.26	3.91
Eu	0.92	3.37	1.21	1.12	2.02	1.27
Gd	3.26	11.4	4.10	3.88	6.90	4.36
Tb	0.544	1.74	0.634	0.750	0.926	0.600
Dy	4.04	9.63	3.62	4.71	5.84	3.79
Ho	0.891	1.71	0.66	1.07	1.02	0.68
Y	2.63	4.50	1.78	2.99	3.55	2.33
Er	25.8	39.0	15.7	29.8	39.2	25.4
Yb	2.65	3.84	1.58	2.93	2.35	1.61
Lu	0.409	0.493	0.211	0.450	0.354	0.243
$^{87}Sr/^{86}Sr$	0.70240	0.70293	0.70291	0.70248	0.70554	0.70500
$^{143}Nd/^{144}Nd$	0.51322	0.51287	0.51288	0.51320	0.51270	0.51271
$^{206}Pb/^{204}Pb$	18.1159	19.588	19.539	18.132	18.959	18.951
$^{207}Pb/^{204}Pb$	15.4629	15.597	15.592	15.468	15.619	15.618
$^{208}Pb/^{204}Pb$	37.681	39.24	39.19	37.75	39.20	39.18